Coherence and chaos in a model of turbulent boundary layer

Xiang Zhou and L. Sirovich
Center for Fluid Mechanics, Turbulence and Computation, Division of Applied Mathematics, Brown University, Providence, Rhode Island 02912

(Received 31 October 1991; accepted 29 July 1992)

The dynamics of coherent structures in the wall region of a turbulent channel flow is considered. The Karhunen–Loève eigenfunctions and Galerkin procedure are used to derive the dynamical description. In a previous treatment of this problem by Aubry *et al.* [J. Fluid Mech. **192**, 115 (1988)] the analysis required an inhomogeneous pressure term to be supplied from outside the theory. In the first part of this paper this theory is reconsidered on the basis of the construction of wall eigenfunctions that have a full channel validity. As a result of the methods developed here, a well-posed Hermitian theory is developed and convergence questions do not arise. Among a number of important consequences is the fact that no exterior pressure is required by the present theory. In the second part of this paper it is shown that the behavior of the resulting model equations include intermittency, quasiperiodic, and chaotic solutions. In the final part of this paper three-dimensional effects are introduced into the dynamics in order to produce a physically more realistic dynamical theory. It is felt that the bursting and ejection events in turbulent boundary layers is given a more satisfactory explanation within this framework.

I. INTRODUCTION

Coherent structures are generally accepted as playing an important role in the wall region of a turbulent boundary layer. The major dynamic behavior of these structures have been described by bursting, ejections, and sweeps.[1–7] Loosely speaking, a *bursting* event consists of a gradual liftup of the longitudinal, streamwise streaks, a sudden oscillation, and a breakup. As a result an *ejection*, i.e., a relatively violent upward motion of low-velocity fluid takes place. Continuity then requires a sweep event that is the compensatory downward motion of high-speed fluid toward the wall. These events are the major contributors to the turbulence-producing process as well as heat transfer near a wall. In this study we model a turbulent boundary-layer flow with a low-dimensional system of ordinary differential equations in order to gain a better understanding of these events.

The Karhunen–Loève (KL) procedure has been used extensively to study coherent structures in a variety of flows[8–17] and related systems.[18] This method has a long history (see Preisendorfer[19] and Sirovich and Everson[20]). It was used by Lorenz,[21] Kutzbach,[22] and Obukhov[23] for analyzing meteorological data, and Lumley[24] suggested that it might provide a rational approach to coherent structures. In this procedure one starts with a known velocity field, which has been obtained either numerically or experimentally, and then calculates the eigenfunctions and the eigenvalues of the two-point correlation kernel formed from the velocity field by time averaging the tensor product of the velocity at two points. The eigenfunctions are used as a basis set to represent the velocity field. Although other basis functions may be used to expand the velocity, the eigenfunctions are optimal, in the sense that the series for the velocity field converges optimally fast by well-defined criteria. The coefficients of the series are time dependent and statistically orthogonal while the eigenvalues themselves are equal to the average kinetic energy of the corresponding modes.

In order to capture the main features of a flow with a low-dimensional dynamical system, one would suppose that a rapidly convergent series for the velocity field is required. This is meant in the sense that the first few modes (i.e., eigenfunctions) should capture most of the kinetic energy. The hope then is that by analyzing the resulting low-dimensional dynamical system in detail we will deepen our understanding of the basic flow mechanisms.

In an experimental study of the flow in the wall region of a turbulent pipe flow, Herzog[5] found that relatively few of the KL modes capture a significant amount of the kinetic energy. On this basis a low-dimensional dynamical description was sought by Aubry *et al.*[25] (henceforth called the Cornell group). They used a low-dimensional model to study the dynamics of the coherent structures in the wall region of a turbulent boundary-layer using the KL eigenfunctions obtained in the pipe flow experiment of Herzog. Due to homogeneity the velocity eigenfunctions factor into Fourier modes in the streamwise and spanwise directions but take on a more complicated form in the wall normal direction. For each mode, one streamwise wave number, k_1, one spanwise wave number, k_3, and one vertical quantum number, q, enter. In this terminology the Cornell model is obtained by truncating the expansion for the velocity so as to include the mode for which $k_1=0$, $q=1$, and $k_3=1,2,3,4,5$. (The Cornell group and Herzog use another terminology different than ours in referring to modes and eigenfunctions.) A low-dimensional system is then derived from the Navier–Stokes equations via the Galerkin projection. The model equations are regarded as

 0899-8213/92/122855-20$04.00

representing the dynamical behavior of the large coherent eddies found in a turbulent boundary layer. Using methods drawn from dynamical systems theory it is shown that the equations exhibit intermittent behavior. This is then related to the bursting events. As a consequence of its derivation, the Cornell model requires the pressure at the outer edge of the boundary layer to appear in the dynamical system (see Sec. III). If this term is neglected they found that the duration between bursts increases without bound, and the Cornell group found it necessary to impose pressure fluctuations in order to preserve bursting. An earlier treatment of the Ginzburg–Landau equation by such a dynamical truncation proved to be highly successful.[11]

The Cornell model neglects the variation in the streamwise direction. In a real turbulent channel flow, the coherent structures observed are fully three dimensional, and thus have streamwise variation. Indeed, turbulence is generally accepted as being an essentially three-dimensional phenomenon. In numerical studies of turbulent channel flow at Reynolds numbers of 3000 and 4250,[26,27] analysis revealed the presence of propagating waves in the turbulent flows, with each propagating wave related to a mode with streamwise variation. This analysis further suggested that the interaction of these waves with the energy bearing streamwise constant modes appears to be essential to the local production of turbulence. The existence of wavelike structures was also found experimentally, by Morrison,[28] for the case of the wall region of fully developed pipe flow over a range of Reynolds numbers. These results suggest that further studies of dynamical systems approximations for well-bounded turbulence should include modes with streamwise variations.

There are three parts in our study. The first part, which concentrates on the formulation, starts with eigenfunctions calculated from a numerical simulation of a channel flow.[3,29] These are used to construct eigenfunctions that are concentrated in the wall region but defined for the full channel. As a result, we are able to present a well-posed formulation in which no inhomogeneous pressure term appears. The second part of our study focuses on five complex ordinary differential equations that form the counterpart in our formulation of the Cornell model. We use an eddy viscosity to reflect the dissipation due to neglected modes. For a range of parameter values our results show intermittency, i.e., the solutions are comprised of spikes, similar to that found for the Cornell model. The third part of our study is motivated by the desire to produce a more realistic three-dimensional model. Since propagating structures were found in a full simulation, it is of interest to see if such structures can exist in a smaller dynamic model. Experimentally, such wavelike structures exist, and the hope is that a low-dimensional model can model such structures. In this context it should be mentioned that Aubry and Sanghi[30] have extended the Cornell model to include three-dimensional modes. From our investigation, we find that the intermittent, quasiperiodic, and chaotic solutions persist as modes with streamwise variations included. Propagating waves that appear in the full simulation are also present in our relatively small dynamic systems. Most importantly, we have confirmed the view that the propagating waves play a more important role to bursting and sweeping events than the pressure fluctuations. We have also examined the power spectra of the reconstructed velocity, we find that the there exist *preferred frequencies*, which appear to be similar to what has been observed in experiments.[31]

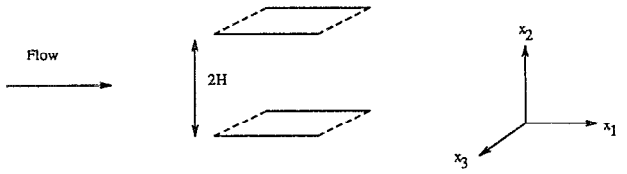

FIG. 1. The geometry of the flow.

II. FORMULATION

In the interest of brevity and clarity the following development is restricted to channel flow. The geometry is that shown in Fig. 1, where the flow is driven by a constant pressure gradient, $-k$. The last can be used to define the friction velocity u_* in the usual way,

$$u_*^2 = kH/\rho, \tag{1}$$

where H is the half channel width. This, in turn, defines the friction Reynolds number

$$\mathrm{Re}_* = Hu_*/\nu = H/l_*, \tag{2}$$

which, as the last expression indicates, can be regarded as the number of wall units, l_*, to the channel centerline.

If velocity is normalized by u_* and distances by H, it then follows that the mean flow equation is given by

$$\frac{d}{dx_2}\overline{u_1u_2} = \frac{1}{R_*}\frac{d^2U}{dx_2^2} + 1, \tag{3}$$

where $\overline{u_1u_2}$ and U are the normalized Reynolds stress and mean velocity, respectively, and x_2, the normalized wall normal coordinate. If perturbed quantities are denoted by lowercase letters, then by using (3) these satisfy

$$\nabla\cdot\mathbf{u} = 0, \tag{4}$$

$$N_i(\mathbf{u}) = \frac{\partial}{\partial t}u_i + U\frac{\partial}{\partial x_1}u_i + \left(u_2U' - \frac{d}{dx_2}\overline{u_1u_2}\right)\delta_{i1} + u_{i,j}u_j + \nabla p - \frac{1}{\mathrm{Re}_*}\nabla^2 u_i = 0, \tag{5}$$

where $U' = dU/dx_2$. In (5) time has been made dimensionless with H/u^* and position by H. In the following we may approximate $\overline{u_1u_2}$ by the spatial average $(1/L_1L_3)\int(u_1u_2)dx_1\,dx_3$, and then calculate $U(x_2)$ by integrating (3) twice.

For purposes of exposition it is useful to postulate the existence of a vector set of orthonormal functions $\{\mathbf{V}^{(n)}(\mathbf{x})\}$, each of which has the divergence-free property (4),

$$\nabla\cdot\mathbf{V}^{(n)}=0. \tag{6}$$

For the moment we turn our back on completeness, boundary conditions, and convergence and expand the velocity field as follows:

$$\mathbf{u}=\sum a_n(t)\mathbf{V}^{(n)}(\mathbf{x}). \tag{7}$$

The coefficients, $a_n(t)$, are determined by projecting along the corresponding direction, $\mathbf{V}^{(n)}$,

$$a_n(t)=(\mathbf{V}^{(n)},\mathbf{u})=\int_V \mathbf{V}^{(n)*}\cdot\mathbf{u}\,d\mathbf{x}, \tag{8}$$

with V the domain of the flow, the asterisk complex conjugation, and the ordinary vector dot product appearing under the integral sign.

The Navier–Stokes equations (5) can be *reduced* by applying the Galerkin procedure to (5) under the expansion (7). In brief, this is obtained by first approximating $\mathbf{u}$ by a finite number of modes chosen from the set, $\{\mathbf{V}^{(n)}\}$. Criteria for distinguishing these modes will be discussed later. If the so distinguished modes are numbered from 1 to N then we write

$$\mathbf{u}\approx\mathbf{u}_N=\sum_{n=1}^{N} a_n(t)\mathbf{V}^{(n)}(\mathbf{x}), \tag{9}$$

and $\mathbf{u}_N$ will be referred to as the projection of $\mathbf{u}$ onto the subspace. Next, the NS equations are projected onto this space,

$$(\mathbf{V}^{(n)},\mathbf{N}(\mathbf{u}_N))=0, \quad n=1,...N. \tag{10}$$

This yields a dynamical system that, in general, is cubic in a_n [since from (3), $\mathbf{U}$ is quadratic in the a_n], has inhomogeneous boundary terms if V is not a domain including both walls of the channel, and ignores projections from outside the distinguished set. We deal with all these issues in the next section.

III. BASIS FUNCTIONS AND BOUNDARY CONDITIONS

For the choice of a basis set we can use the KL procedure to determine the empirical eigenfunctions. This approach was first used with remarkable success for the Ginzburg–Landau equation[11] and later improved on.[32] It was also used in order to create a model of intermittency for the turbulent boundary layer by the Cornell group. To obtain this basis set we first form the correlation matrix

$$K_{ij}(\mathbf{x},\mathbf{y})=\langle u_i(\mathbf{x})u_j(\mathbf{y})\rangle, \tag{11}$$

where angle brackets indicate a time average. The eigenfunctions are then determined by

$$\int_V K_{ij}(\mathbf{x},\mathbf{y})V_j(\mathbf{y})d\mathbf{y}=\lambda V_i(\mathbf{x}). \tag{12}$$

The set so generated forms a complete orthonormal set over the domain V, under the reasonable assumption of the square integrability of $\mathbf{u}$. The resulting eigenfunctions then have optimal convergence properties.[33] (See Aubry[34] and Sirovich and Everson[21] for a recent review of the KL procedure.)

As a result of homogeneity in the streamwise, x_1, and spanwise, x_3, directions it follows that the empirical eigenfunctions are sinusoidal in these directions, and that they have the factorable form

$$V_j^{(n)}=\psi_j^{(n)}(\mathbf{k},x_2)\exp\left[2\pi i\left(\frac{k_1x_1}{L_1}+\frac{k_3x_3}{L_3}\right)\right], \tag{13}$$

where the wave number $\mathbf{k}=(k_1,k_3)$ and q is the vertical quantum number. The latter indexes the vertical part of the eigenfunctions and L_1 and L_3 denote the streamwise and spanwise dimensions of the periodic box in which the turbulent flow takes place. Further properties of the empirical eigenfunctions that bear mention is that they are divergence-free,

$$\nabla\cdot\mathbf{V}^{(n)}=0, \tag{14}$$

for all n, a property that follows from (4). In addition,

$$\mathbf{V}^{(n)}(x_2=0)=0=\mathbf{V}^{(n)}(2), \tag{15}$$

which follows from the boundary conditions on $\mathbf{u}$.

A. Review of the Cornell model

In their approach the Cornell group focuses attention on the region near the wall, given by

$$V_w\colon\ 0\leqslant x_2^+=x_2/l_*\leqslant 42; \quad -\infty<x_1, \quad x_3<\infty, \tag{16}$$

where we follow customary practice and measure the distance from the wall in wall units x_2^+. This includes the buffer zone. We regard this as being of nominal extent and for purposes of comparison we will use the same region in our deliberations. To obtain dynamical equations, as outlined in Sec. II, we substitute the expression (13) for $\mathbf{V}^{(n)}$ in (9) and this into (5), and thus consider

$$(\mathbf{V}^{(n)},\mathbf{N}(\mathbf{u}))_{V_w}=\int_{V_w}\mathbf{V}^{(n)*}\cdot\mathbf{N}(\mathbf{u})d\mathbf{x}=0, \quad n=1,\ldots. \tag{17}$$

The functions $\mathbf{V}^{(n)}$ that appear in (17) are those obtained from the KL procedure, (12) applied to the restricted domain (16). To distinguish these from the full channel eigenfunction we henceforth use a circumflex, $\{\hat{\mathbf{V}}^{(n)}\}$ to denote the wall eigenfunctions, and formally write

$$\mathbf{u}=\sum \hat{a}_n(t)\hat{\mathbf{V}}^{(n)}(x). \tag{18}$$

For example, the time derivative appearing in (17) yields

$$\left(\hat{\mathbf{V}}^{(n)},\frac{\partial \mathbf{u}}{\partial t}\right)_{V_w}=\frac{\partial \hat{a}_n}{\partial t}, \tag{19}$$

where the subscript N has been temporarily neglected.

As mentioned earlier, a pressure inhomogeneity arises. To see this, consider the pressure term of (17),

$$(\hat{\mathbf{V}}^{(n)},\nabla p)_{V_w}=\int_{V_w}\hat{\mathbf{V}}^{(n)*}\cdot\nabla p\,d\mathbf{x}=\int_{V_w}\nabla\cdot(\hat{\mathbf{V}}^{(n)*}p)d\mathbf{x}. \tag{20}$$

The last is obtained since the eigenfunctions are divergence-free. From periodicity and the vanishing of $\mathbf{V}^{(n)}$ at $x_2=0$, we obtain

$$(\hat{\mathbf{V}}^{(n)},\nabla p)_{V_w}=\int_{x_2^+=42}\hat{V}_2^{(n)*}p\,dx_1\,dx_3\,, \tag{21}$$

which indicates that the fluctuating pressure must be supplied at the outer (geometrical) boundary of V_w, viz., $x_2^+=42$.

There is another, related, feature of the Cornell approach that merits attention, and we illustrate it by considering the viscous contribution to (17), viz.,

$$(\hat{\mathbf{V}}^{(n)},\nabla^2\mathbf{u})_{V_w}=\int_{V_w}\hat{\mathbf{V}}^{(n)*}\cdot\nabla^2\mathbf{u}\,d\mathbf{x}. \tag{22}$$

In the Cornell approach this is evaluated by taking the projection

$$\mathbf{u}_N=P_N\mathbf{u}=\sum_{n=1}^{N}\hat{a}_n(t)\hat{\mathbf{V}}^{(n)}(\mathbf{x}), \tag{23}$$

and substituting (23) directly into the right-hand side of (22) for $\mathbf{u}$, so that

$$(\hat{\mathbf{V}}^{(m)},\nabla^2\mathbf{u}_N)\approx\sum_{n=1}^{N}\hat{a}_n(\hat{\mathbf{V}}^{(m)},\nabla^2\hat{\mathbf{V}}^{(n)}), \tag{24}$$

or equivalently by writing

$$\nabla^2\mathbf{u}_N=\sum_{n=1}^{N}\hat{a}_n\nabla^2\hat{\mathbf{V}}^{(n)}. \tag{25}$$

Term by term, differentiation is taken for granted.

The approach described above places no restriction on the fluid velocity at the upper (fictitious) boundary of $x_2^+=42$. The customary three conditions on $\mathbf{u}$ at a boundary have been replaced by a single boundary condition, viz., p given on the boundary. This we claim produces an ill-posed problem. To illustrate this in simple terms, consider the related problem of fluid flow in a slab say, V_s: $x_u\geqslant x_2\geqslant x_l$. If we carry over the recipe used by the Cornell group to this problem the implication is that we can solve the NS equations in the slab by prescribing the pressure on the boundaries of the slab. As an example of this formatting of the flow problem, consider the Stokes problem, which may be regarded as a special case of the general problem,

$$\nabla\cdot\mathbf{u}=0 \tag{26}$$

$$\frac{\partial \mathbf{u}}{\partial t}+\nabla p=\frac{1}{R_*}\nabla^2\mathbf{u}, \tag{27}$$

for $\mathbf{x}\in V_s$ and p given on ∂V_s. On taking the divergence of the momentum equation (27), we obtain

$$\nabla^2 p=0. \tag{28}$$

Since p is given on ∂V_s, p is therefore determined in V_s. This still leaves us with the problem of finding the solution, $\mathbf{u}$, to (27) with ∇p now regarded as a known function. As elementary considerations demonstrate, this is not a solvable problem without the prescription of boundary conditions for the velocity, $\mathbf{u}$.

These deliberations cast doubt on the convergence of the term-by-term differentiated series (25). In Foias *et al.*,[35] it is demonstrated that the series expansion for $\mathbf{u}(\mathbf{x},t)$ (9) in terms of the empirical eigenfunction is rapidly convergent. In fact for $n\uparrow\infty$ the coefficients descend to zero, on average, exponentially with n. In this case term-by-term differentiation is permitted. (The above discussion is not contradicted since each $\mathbf{V}^{(n)}$ satisfies the correct boundary conditions.)

It is of interest to point out that the basis of the exponential falloff estimates comes from the study of the Stokes eigenfunction theory. Since, as we just showed, the Stokes problem is ill posed, no comparable *a priori* estimate can be given for the wall (or slab) expansion.

Generally, in cases where the convergence of a development is in question, it is prudent to use a transform approach rather than a series development. In regard to the dissipative term this entails, replacing it by

$$(\hat{\mathbf{V}}^{(n)},\nabla^2\mathbf{u})_{V_u}=(\nabla^2\mathbf{V}^{(n)},\mathbf{u})_{V_w}+B^+(\mathbf{u},\nabla\mathbf{u}), \tag{29}$$

where the linear term

$$B^+=\int_{x_2^+=42}\left(\hat{\mathbf{V}}^{(n)*}\cdot\frac{\partial}{\partial x_2}\mathbf{u}-\mathbf{u}\cdot\frac{\partial}{\partial x_2}\hat{\mathbf{V}}^{(n)*}\right)dx_1\,dx_3\,, \tag{30}$$

represents the contribution from the boundary, and from which it is clear that an appropriate combination of $\mathbf{u}$ and its derivatives must be specified on the boundary.

As (29) clearly indicates, the Laplace operator is clearly not Hermitian if the wall zone is considered. Formatting the development in the form shown in (29) is more forgiving in regard to the convergence issue and clearly indicates the need for boundary terms. However, it is not clear that this alteration in the procedure will lead to convergence. As is well known the slow convergence of the Laplacian [The left-hand side of (29)] is improved upon if the right-hand side of (29) is used.

In the next section we present a formulation that focuses on the wall region, is well posed and Hermitian, and

avoids the convergence issues that have been raised. In all cases relatively few modes enter, and the question of convergence should not be a genuine concern. On the other hand, the issue of the presence of a pressure term takes on a conceptual importance.

IV. ALTERNATIVE WALL EIGENFUNCTIONS

We now present an alternative approach that not only concentrates attention on the wall region but also avoids the difficulties raised in the previous section. In brief, we introduce a linear transformation T of the full channel eigenfunctions so that they represent the wall eigenfunctions in the wall region,

$$\hat{\mathbf{V}}^{(n)}(\mathbf{x})=\sum_m T_{nm}\mathbf{V}^{(m)}(\mathbf{x}). \tag{31}$$

Note that we use the same notation as earlier for the wall eigenfunctions, even though these now have a full channel interpretation. Since this is the case we can use the full channel inner product. From this it follows that (1) no inhomogeneous pressure appears, and therefore (2) ∇^2 is Hermitian under the inner product. To specify the transformation T_{nm} we begin with the observation that the full channel eigenfunctions have the form of (13), and from this that the wall eigenfunctions must have a similar form,

$$\hat{V}_j^{(n)}=\phi_j^{(n)}(k_1,k_3,x_2)\exp[2\pi i(k_1x_1/L_1+k_3x_3/L_3)], \tag{32}$$

since translational invariance is still applicable. Substitution of (13) and (32) into (31) yields

$$\phi_j^{(n)}(k_1,k_3,x_2)=\sum_m T_{nm}\psi_j^{(m)}(k_1,k_3,x_2). \tag{33}$$

The two sets of eigenfunctions satisfy the equations

$$\int_0^2 K_{ij}(k_1,k_3,x_2,x_2')\psi_j^{(n)}(k_1,k_3,x_2')dx_2' =\Lambda^{(n)}(k_1,k_3)\psi_i^{(n)}(k_1,k_3,x_2) \tag{34}$$

and

$$\int_0^\delta K_{ij}(k_1,k_3,x_2,x_2')\phi_j^{(n)}(k_1,k_3,x_2')dx_2' =\lambda^{(n)}(k_1,k_3)\phi_i^{(n)}(k_1,k_3,x_2), \tag{35}$$

respectively. Here δ is the thickness of the wall layer, which, according to (16), is taken to be 42 wall units. The kernel K_{ij} is given by

$$K_{ij}(k_1,k_3,x_2,x_2')=\langle\hat{u}_i(k_1,k_3,x_2)\hat{u}_j^*(k_1,k_3,x_2')\rangle. \tag{36}$$

The angle brackets indicate an ensemble average and the asterisk indicates a complex conjugation. The Fourier transformed velocities are given by

$$\hat{u}_i^{(m)}(k_1,k_3,x_2)=\sum_{x_1}\sum_{x_3}u_i^{(m)}(x_1,x_2,x_3) \times\exp[2\pi i(k_1x_1/L_1+k_3x_3/L_3)], \tag{37}$$

where the superscript denotes the sampling times,

$$u_i^{(m)}(x_1,x_2,x_3)=u_i(x_1,x_2,x_3,m\Delta t), \tag{38}$$

so that the ensemble average of a typical quantity is given by

$$\langle u\rangle=\frac{1}{M}\sum_{n=1}^{M}u^{(n)}, \tag{39}$$

where M denotes the number of members in the ensemble.

To find the equation for T_{nm}, we appeal to the spectral decomposition of the kernel K_{ij} (Mercer's theorem[36]),

$$K_{ij}(k_1,k_3,x_2,x_2')=\sum_l \Lambda^{(l)}\psi_i^{(l)}(k_1,k_3,x_2)\psi_j^{(l)*}(k_1,k_3,x_2'). \tag{40}$$

This may be truncated in view of the very rapid falloff in $\Lambda^{(l)}$ (see Foias *et al.*[35] for an argument that these vanish exponentially) and substitute this and (33) into (35), to obtain

$$\sum_l \psi_i^{(l)}(x_2)\left[\sum_m\left(\Lambda^{(l)}\int_0^\delta \psi_j^{(l)*}(x_2')\psi_j^{(m)}(x_2')dx_2'\right)\right]T_{nm} =\lambda^{(n)}\sum_l T_{nl}\psi_i^{(l)}(x_2). \tag{41}$$

This equation is valid for the entire channel, over which $\{\psi_j^{(l)}(x_2)\}$ are orthonormal, thus we obtain an eigenvalue problem for T_{nm},

$$\Lambda^{(l)}\sum_m G_{lm}T_{nm}=\lambda^{(n)}T_{nl}, \tag{42}$$

where

$$G_{lm}=\int_0^\delta \psi_j^{*(l)}(x_2')\psi_j^{(m)}(x_2')dx_2'. \tag{43}$$

In matrix notation, (42) can be written as the eigenproblem

$$\mathbf{\Lambda G t}^{(n)}=\lambda^{(n)}\mathbf{t}^{(n)}, \tag{44}$$

where $\mathbf{\Lambda}$ is the diagonal matrix with entries $\Lambda^{(l)}$ and $T_{nl}=t_l^{(n)}$. The problem can be symmetrized under the transformation

$$\mathbf{t}=\mathbf{\Lambda}^{1/2}\mathbf{s},$$

i.e.,

$$\mathbf{\Lambda}^{1/2}\mathbf{G}\mathbf{\Lambda}^{1/2}\mathbf{s}=\lambda\mathbf{s}. \tag{45}$$

In view of the rapid falloff to zero of $\Lambda^{(l)}$, we can comfortably truncate the infinite eigenvector problem posed by

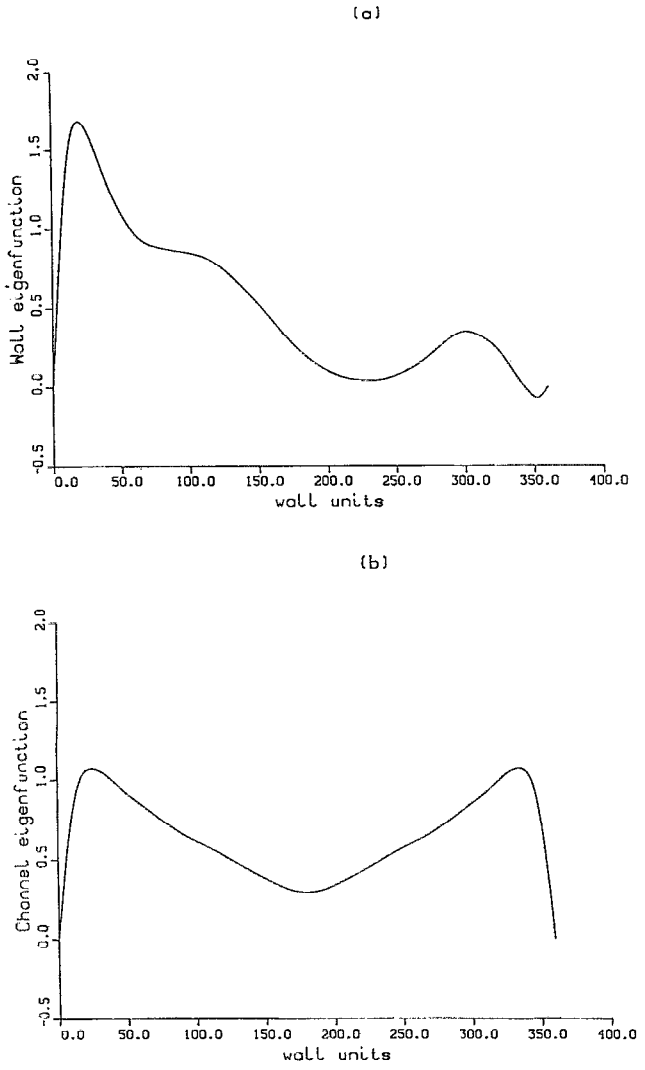

FIG. 2. A comparison of a channel eigenfunction and a wall eigenfunction, the streamwise component, $k_1=0$, $k_3=1$, $q=1$. (a) Wall eigenfunction; (b) channel eigenfunction.

(45) [for each pair (k_1,k_3)]. In our calculations we took $\mathbf{G}$ to be a 32×32 matrix. Choosing larger matrices produced corrections of less than $O(10^{-6})$. Inversely, if we go from a 16×16 matrix to the 32×32 case the wall eigenfunctions change $O(10^{-4})$.

It is important to keep in mind that in fitting a wall eigenfunction by 32 full channel eigenfunctions this is done for each wave number pair. For example, for the system of 16 complex modes that we consider later, roughly 2^{10} full channel eigenfunctions are used to represent the wall eigenfunctions.

Figures 2(a) and 2(b) show examples of a full channel eigenfunction and the analogous wall eigenfunction.

V. EMPIRICAL DYNAMIC EQUATIONS AND SYMMETRY CONSIDERATIONS

To derive the dynamic equations we follow the procedure outlined in Secs. II and III. We use the wall eigenfunctions (31) developed in the last section as basis functions and apply the Galerkin projection across the entire channel. In particular, we write

$$\mathbf{u}_N=\sum_{n,\mathbf{k}} a_{\mathbf{k}}^{(n)}(t)\hat{\mathbf{V}}^{(n)}(\mathbf{k},\mathbf{x}), \tag{46}$$

where $\mathbf{k}=(k_1,k_3)$ and

$$\hat{V}_j^{(n)}=\phi_j^{(n)}(\mathbf{k},x_2)\exp\left[2\pi i\left(\frac{k_1x_1}{L_1}+\frac{k_3x_3}{L_3}\right)\right]. \tag{47}$$

The Galerkin procedure is then given by

$$\begin{aligned}(\hat{\mathbf{V}}^{(n)},\mathbf{N}(\mathbf{u}_N))&=\int_0^{L_3}\int_0^{L_1}\int_0^2 N_j(\mathbf{u}_N)\phi_j^{(n)*}\exp[-2\pi i(k_1x_1/L_1\\&\quad+x_3/L_3)]dx_2\,dx_1\,dx_3=0,\end{aligned} \tag{48}$$

where N_j is the Navier–Stokes operator (5) and $j=1,2,3$. From (48) we then obtain the following dynamical system:

$$\begin{aligned}\sum_m g_{nm}(\mathbf{k})\frac{da_{\mathbf{k}}^{(m)}}{dt}&=\sum_m L(m,n,\mathbf{k},\mathrm{Re}_*)a_{\mathbf{k}}^{(m)}\\&\quad+\sum_{p,q}\sum_{\mathbf{k}'}Q(p,q,\mathbf{k}',n,\mathbf{k})a_{\mathbf{k}'}^{(p)}a_{\mathbf{k}-\mathbf{k}'}^{(q)}\\&\quad-\mathrm{Re}_*\sum_{p,q,r}\sum_{\mathbf{k}'}C(p,q,r,\mathbf{k}',n,\mathbf{k})a_{\mathbf{k}}^{(r)}a_{\mathbf{k}'}^{(p)}a_{\mathbf{k}'}^{(q)*},\end{aligned} \tag{49}$$

with coefficients

$$g_{nm}(\mathbf{k})=\int_0^2\phi_i^{(m)}(\mathbf{k})\phi_i^{(n)*}(\mathbf{k})dx_2\,, \tag{50}$$

here and in the following, the argument x_2 is suppressed in the ϕ_j's,

$$L(m,n,\mathbf{k},\mathrm{Re}_*)=L^{(1)}(m,n,\mathbf{k},\mathrm{Re}_*)+L^{(2)}(m,n,\mathbf{k},\mathrm{Re}_*), \tag{51}$$

$$\begin{aligned}L^{(1)}(m,n,\mathbf{k},\mathrm{Re}_*)&=\left\{-g_{mn}(\mathbf{k})\left[\left(\frac{2\pi k_1}{L_1}\right)^2+\left(\frac{2\pi k_3}{L_3}\right)^2\right]\right.\\&\quad\left.+\int_0^2 D^2\phi_i^{(m)}(\mathbf{k})\phi_i^{(n)*}(\mathbf{k})dx_2\right\}(\mathrm{Re}_*)^{-1},\end{aligned} \tag{52}$$

$$L^{(2)}(m,n,\mathbf{k},\mathrm{Re}_*)$$

$$=\mathrm{Re}_*\int_0^2\left((x_2-1)\phi_2^{(m)}(\mathbf{k})\phi_1^{(n)*}(\mathbf{k})\right.$$

$$\left.-\frac{2\pi ik_1}{L_1}\frac{x_2(2-x_2)}{2}\phi_i^{(m)}(\mathbf{k})\phi_i^{(n)*}(\mathbf{k})\right)dx_2\,, \tag{53}$$

$$Q(p,q,\mathbf{k}',n,\mathbf{k})=-(1-\delta_{\mathbf{k}0})\int_0^2\phi_j^{(p)}(\mathbf{k}')\Omega_j(\mathbf{k}-\mathbf{k}')$$

$$\times\phi_i^{(q)}(\mathbf{k}-\mathbf{k}')\phi_i^{(n)*}(\mathbf{k})dx_2\,, \tag{54}$$

$$C(p,q,r,\mathbf{k}',n,\mathbf{k})$$

$$=\int_0^2\phi_1^{(p)}(\mathbf{k}')\phi_2^{(q)*}(\mathbf{k}')\phi_1^{(n)*}(\mathbf{k})\phi_2^{(r)}(\mathbf{k})dx_2$$

$$+\frac{2\pi ik_1}{L_1}\int_0^2\phi_i^{(n)*}(\mathbf{k})\phi_i^{(r)}(\mathbf{k})\int_0^{x_2}\phi_1^{(p)}(\mathbf{k}')$$

$$\times\phi_2^{(q)*}(\mathbf{k}')dx_2'\,dx_2\,, \tag{55}$$

here $\Omega_j(\mathbf{k}-\mathbf{k}')=2\pi i(k_j-k_j')/L_j$ if $j=1,3$, and $\Omega_2(\mathbf{k}-\mathbf{k}')=D=d/dx_2$.

The system (49) can be reduced on the basis of physical symmetries of the flow. In particular,

$$a_{-\mathbf{k}}^{(n)}=a_{\mathbf{k}}^{(n)*} \tag{56}$$

and

$$\phi_j^{(n)}(-\mathbf{k})=\phi_j^{(n)*}(\mathbf{k}), \tag{57}$$

since the velocity is real valued. Since the flow is invariant under streamwise and spanwise translations, $x_j\to x_j+\alpha_j$, $j=1,3$, it follows that the dynamical system (49) is invariant under the rotational transformations,

$$a_{\mathbf{k}}^{(n)}\to a_{\mathbf{k}}^{(n)}\exp(ik_1\alpha_1+ik_3\alpha_3). \tag{58}$$

The problem also remains invariant under spanwise reflection:

$$(x_1,x_2,x_3,u_1,u_2,u_3)\to(x_1,x_2,-x_3,u_1,u_2,-u_3), \tag{59}$$

and we find that[10]

$$\phi_j^{(n)}(k_1,-k_3)=I_j\phi_j^{(n)}(k_1,k_3), \tag{60}$$

where $I_1=I_2=1$, $I_3=-1$. This leads to the invariance of (49) under

$$a_{\mathbf{k}}^{(n)}\to a_{(k_1,-k_3)}^{(n)}. \tag{61}$$

To see this we use relation (60), and can show that

$$L(m,n,\mathbf{k}^*,\mathrm{Re}_*)=L(m,n,\mathbf{k},\mathrm{Re}_*), \tag{62}$$

$$Q(p,q,\mathbf{k}'^*,n,\mathbf{k}^*)=Q(p,q,\mathbf{k}',n,\mathbf{k}), \tag{63}$$

$$C(p,q,r,\mathbf{k}'^*,n,\mathbf{k}^*)=C(p,q,r,\mathbf{k}',n,\mathbf{k}). \tag{64}$$

Here $\mathbf{k}^*=(k_1,-k_3)$. Thus Eq. (49) is invariant under (61) and reflection symmetry is maintained.

VI. LOW-DIMENSIONAL MODEL EQUATIONS

To model a real flow by a low-dimensional system requires ignoring all but a few modes. This has the effect of neglecting the dissipative drain of the missing modes. It should be clear that without this energy sink the retained modes will behave far too energetically, a state of affairs that is typical in insufficiently resolved numerical simulations. Usually this is accounted for, at least qualitatively, by the introduction of an eddy viscosity model, which assumes that the higher-order stress is proportional to the lower-order rate of strain,

$$\tau_{ij}^{>}=-e(u_{i,j}^{<}+u_{j,i}^{<}). \tag{65}$$

The proportionality constant e, is the *eddy viscosity*. Here $<$ denotes the sum over all resolved modes (k_1,k_3,n), such that $|k_1|\leqslant k_{1c}, |k_3|\leqslant k_{3c}$, $n\leqslant n_c$; and $>$ denotes the sum over all the modes (k_1,k_3,n), such that $|k_1|>|k_{1c}|$ or $|k_3|>k_{3c}$ or $n>n_c$, where (k_{1c},k_{3c},n_c) marks the cutoff mode.

This is analogous to the approach by the Cornell group, who introduce the eddy viscosity through the Heisenberg energy transfer model. They then relate the eddy viscosity to the cutoff eigenvalue. However, a free parameter is still on the loose. The resulting equations, shown below, are the same in both instances and for the full formal treatment we refer to the work by the Cornell group.

In order to facilitate comparisons with the results of the Cornell group, we adopt the severe truncation chosen by them, viz., $n=1$, $\mathbf{k}=(0,k)$ in Eq. (46). For this specific truncation, there is only one nonzero index $k_3=k$ in $\mathbf{k}$ and $g_{mn}(\mathbf{k})=g_{11}(\mathbf{k})=1$. On letting $A_k=a_{\mathbf{k}}^1$, we have

$$\frac{dA_k}{dt}=L(k,\mathrm{Re}_*)A_k+\sum_{k'}Q_{k',k-k'}A_{k'}A_{k-k'}$$

$$-\mathrm{Re}_*\sum_{k'}C(k',k)A_k|A_k|^2, \tag{66}$$

where $k=1,2,\ldots,5$, $A_{-k}=A_k^*$, and

$$L(k,\mathrm{Re}_*)=L^{(2)}(k,\mathrm{Re}_*)+(1+e)L^{(1)}(k,\mathrm{Re}_*), \tag{67}$$

$L^{(2)}(k,\mathrm{Re}_*)>0$ is the driving term, proportional to Re_*, $L^{(1)}(k,\mathrm{Re}_*)<0$ is the damping term, proportional to $1/\mathrm{Re}_*$, and e comes from the eddy viscosity model. In what follows we will keep Re_* fixed but vary e.

An additional symmetry in the reduced equation (66) resides in the coefficient matrix for cubic terms. This follows from

$$C(k,k')=\int_0^2\phi_1^{(1)}(k')\phi_2^{(1)*}(k')\phi_1^{(1)*}(k)\phi_2^{(1)}(k)dx_2\,. \tag{68}$$

It is straightforward to see that $C(k,k')$ is Hermitian. Further, since $k_1=0$, we can deduce from (57) and (60) that $\phi_j^{(q)}(\mathbf{k})$ $(j=1,2)$ has to be real to satisfy the spanwise reflection symmetry.[9,10] Therefore, $C(k,k')$ is real symmetric. To see that this symmetry does not depend on the normalization of the eigenfunctions, we consider

$$\phi_j^{(q)}(\mathbf{k}) \to \alpha^{(q)}(\mathbf{k})\phi_j^{(q)}(\mathbf{k}), \tag{69}$$

where $\alpha^{(q)}(\mathbf{k})$ represents normalization constants. It then follows that

$$C(k,k') \to (\alpha_k^{(1)}\alpha_{k'}^{(1)})^2 C(k,k'), \tag{70}$$

which remains symmetric.

VII. NUMERICAL STUDIES OF THE FIVE-MODE MODEL EQUATIONS

We have carried out a careful and extensive numerical integration of our five-mode model equations and have found that they display intermittent, quasiperiodic, and chaotic behavior. The results are briefly summarized in Table I.

TABLE I. Results of our five-mode model equations.

Eddy viscosity	Behavior
$14.0 \geqslant e \geqslant 4.6$	Intermittency
$4.5 \geqslant e \geqslant 4.1$	Transition from intermittency to quasiperiodic solution
$4.2 \geqslant e > 2.2$	Quasiperiodic solutions, chaos
$2.1 \geqslant e \geqslant 0$	Equilibrium, periodic, quasiperiodic, and chaotic solutions

It should be noted that the five-mode model is only composed of roll-like structures aligned in the streamwise direction. Thus, the amplitudes governed by the five-mode equations describe what is happening to the admixture of these *rolls*. In essence, we are observing spanwise shifts of the rolls.

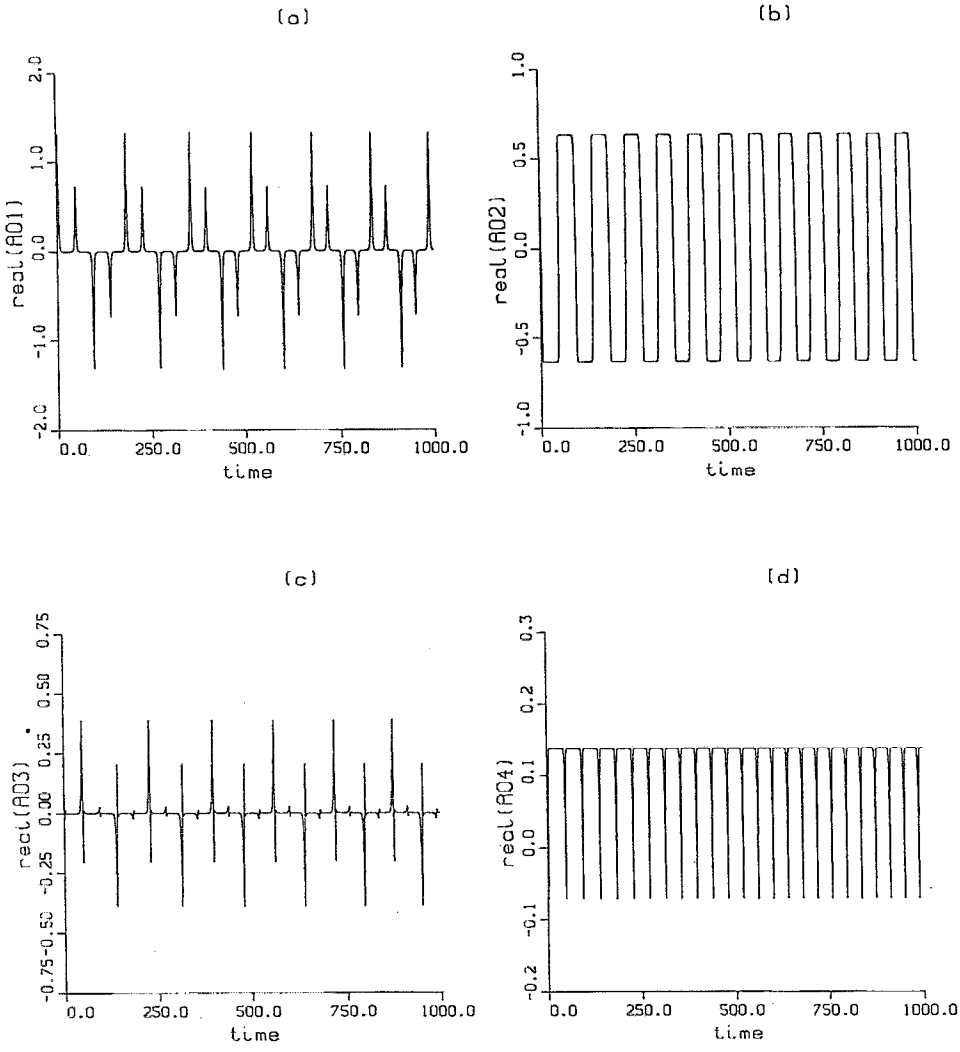

FIG. 3. Regular intermittency, five modes, $e=4.6$. (a) real(A_1); (b) real(A_2); (c) real(A_3); and (d) real(A_4).

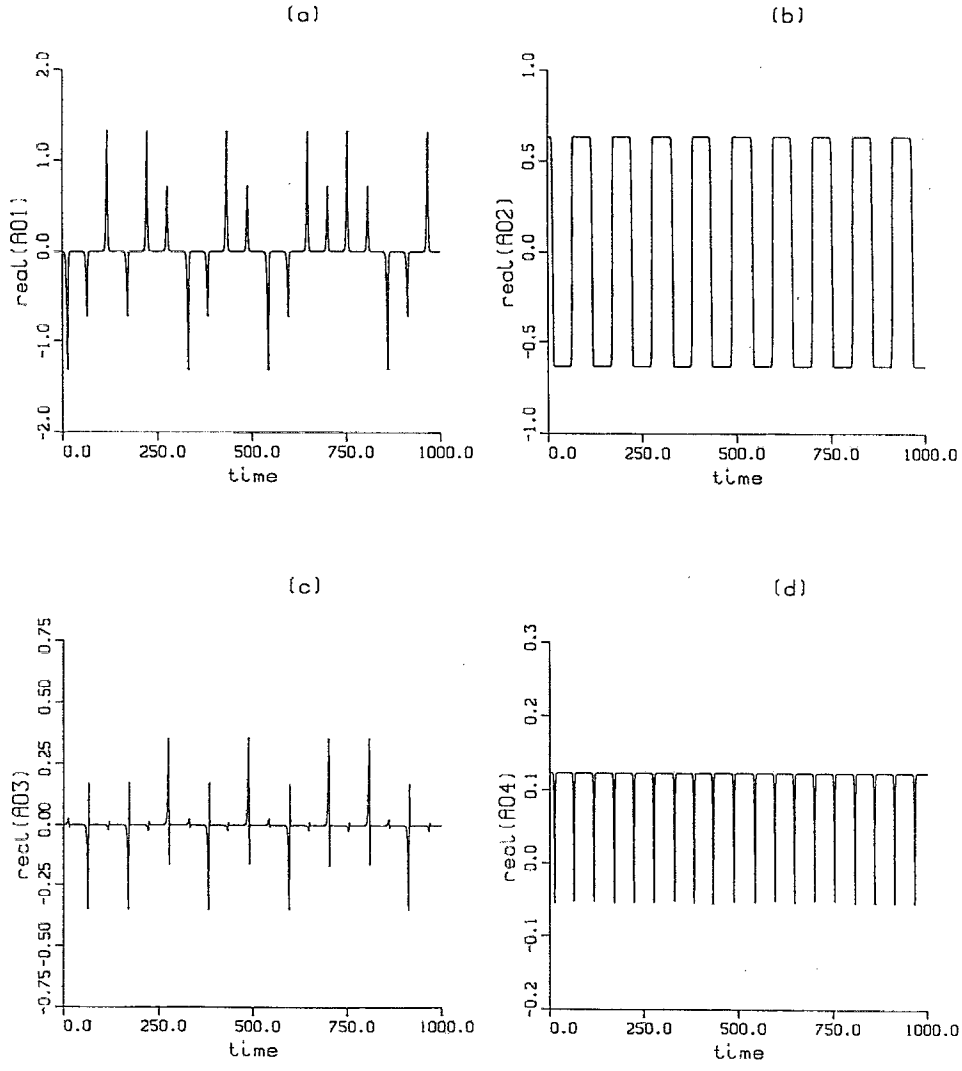

FIG. 4. Irregular intermittency, five modes, $e=5$. (a) real(A_1); (b) real(A_2); (c) real(A_3); and (d) real(A_4).

Equation (66) can display two types of intermittent solutions for $4.6 \leqslant e \leqslant 14$. (For large e, the system is frozen to the steady state.) The first of these we call regular and is shown in Fig. 3. The second, which we call irregular, is shown in Fig. 4. The distinction between the two classes can be seen in the time histories of the A_1 mode. The time traces of A_1 are comprised of short and tall spikes falling above and below the null state. If we characterize by $+1$ a positive spike and by -1 a negative spike, then we have a periodic sequence $\{...,1,1,-1,-1,1,1,-1,-1,...\}$ in the regular case, and an aperiodic sequence $\{...,1,-1,-1,-1,1,1,-1,1,...\}$ in the irregular case. The actual solution in the regular case need not be periodic, although it is the case shown in Fig. 3. Whether the intermittency is regular or irregular depends on the parameter e, and the initial conditions. Otherwise stated, regular and irregular spike solutions have different basins of attractions. Figure 5(a) shows the interspike intervals for a regular spike solution and Fig. 5(b) shows this for an irregular solution. The parameter e is the same for both these figures, but the initial conditions are different. Clearly the regular solution is not periodic in this case.

Equation (66) exhibits quasiperiodic and chaotic solutions when $2.2 \leqslant e \leqslant 4.2$. A transition from quasiperiodic to a chaotic solution is shown in Fig. 6. For two torus motion the situation can be conveniently viewed in three space. For this reason we have chosen to look at the three components of fluid velocity at some fiducial point, the location of which is unimportant. Since this carries more physical content than viewing the amplitudes, we will continue to adopt this picture, when possible, in what follows. As we see in Fig. 6 the quasiperiodic solutions appear on a twisted torus. As the parameter, e, changes, the torus becomes *fat* and can rotate by 180°, and collapses before chaos sets in. For each torus in Figs. 6(a)–6(c), there are just two frequencies: f_1 and f_2. For each frequency, f, in the power spectrum of such solutions, there are integers (n_1,n_2), such that $f=n_1f_1+n_2f_2$, but the frequencies (f_1,f_2) change with the tori. The power spectra shift as a torus is stretched

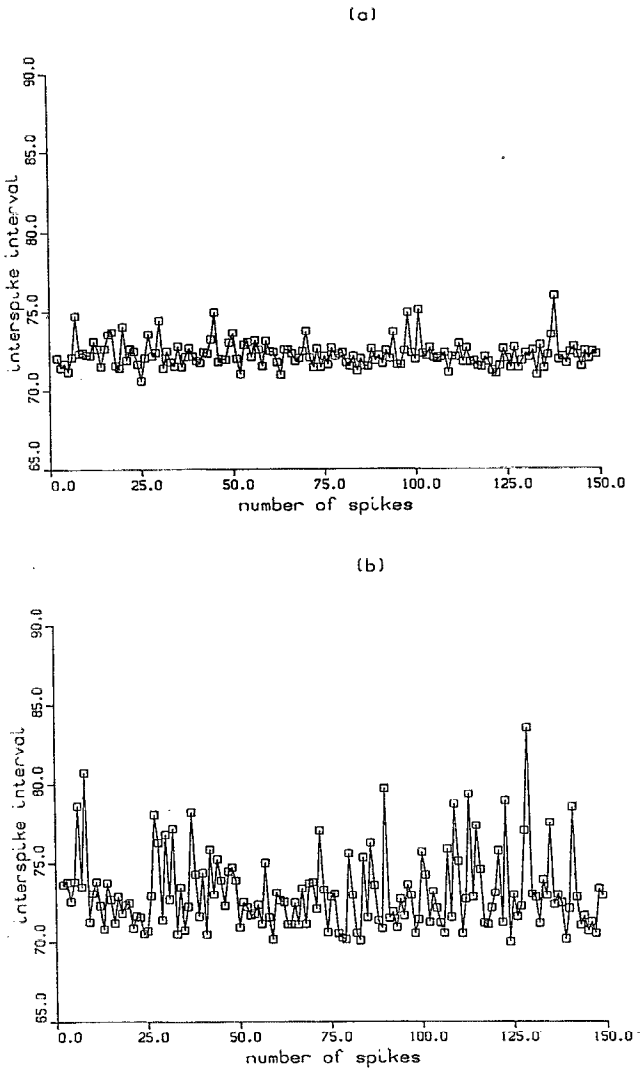

FIG. 5. The interspike intervals for the regular and irregular intermittency at one parameter $e=14$, five modes. (a) Regular one, initial conditions are (0.4,0.8), $(-0.5,0.19)$, $(0.78,-1.2)$, $(-0.34,1.3)$, and (1.1,0.3); (b) irregular one.

or rotated. Chaos appears to result from an unstable two-frequency quasiperiodic solution.

The full range of solutions becomes quite complicated for $0 \leqslant e \leqslant 2.1$. We find equilibrium, periodic, quasiperiodic, and chaotic solutions. These solutions depend on the eddy viscosity e and on initial conditions. An interesting transition occurs at $e=1.383\,33$. At this value we find a steady-state solution going into a quasiperiodic solution. Therefore, there appears to be a double-Hopf bifurcation, i.e., two pair of complex eigenvalues simultaneously crossing the imaginary axis. The same initial conditions in Fig. 5(a) are chosen.

A. Heteroclinic loop and effect of noise

The solutions shown in Figs. 3–5 bear some similarity to those found by the Cornell group, who suggest that a heteroclinic loop accompanied by noise is responsible for this behavior. In two subsequent studies, the equations for the two spanwise modes A_1 and A_2 were investigated in greater detail,[37] and the concept of "noise induced intermittency" was introduced.[38]

For purposes of further discussion, we demonstrate here how a heteroclinic loop is involved in the problem. (For full discussions of heteroclinic loops see Guckenheimer and Holmes[39] and Wiggens.[40]) Equation (66) has equilibria for $|A_i| = \text{const} \neq 0$, with $i=2,4$ and $A_j=0$ with $j=1,3,5$. These equilibria are saddle points having one positive and eight negative eigenvalues. Due to the rotational symmetry, there is also a zero eigenvalue. Corresponding to these eigenvalues there are unstable, stable, and center manifolds respectively. Suppose there exists a stable heteroclinic loop, which consists of cycles connecting two of the equilibria, then asymptotically, a solution will remain close to the heteroclinic loop if no other stable solutions are present. The solution then stays close to the stable manifold of one equilibrium point for some time and runs away from the neighborhood of the equilibrium point along the unstable manifold of that point. The solution then is attracted close to the stable manifold of the other equilibrium point, and then undergoes similar behavior. Figure 7(a) shows a heteroclinic loop. When the solution runs away from the neighborhood of the unstable manifolds of the equilibria, spikes appear. Since there are two opposite directions on an unstable manifold, the spikes on the time history can be above or below the null state. As before, we have plotted the three components of velocity in Figs. 7(a)–7(d) and the curves that are seen result from the numerical integration. For the periodic case the curves have *no thickness*. However, as tori set in the curves *thicken*.

Our current study confirms that noise can have an important influence on a stable heteroclinic loop. For example, the regular intermittency obtained with $O(10^{-12})$ precision becomes irregular if the precision is reduced to $O(10^{-9})$. However, the existence of regular spike solutions suggest that the role of noise needs further investigation. If it were always noise that triggered a spike when a solution is near to an equilibrium point, it would push the solution randomly to either one of the two opposite directions of the unstable manifold, and only irregular spike solutions on the time traces would be seen. Obviously, this is not the case. Since it is our contention that some neglected mode with streamwise variations, which lie high above the noise floor, actually dominate the triggering process, whether spikes in our solutions are triggered by noise is not important.

VIII. A DISCUSSION OF THE ORIGIN OF THE BURSTS

The Cornell group suggest that the intermittent solutions of their five complex modes are related to bursts that are seen in the boundary layer. In the course of their study they found that the burst (spike) interval increases without bound, but if a small disturbance is introduced (e.g.,

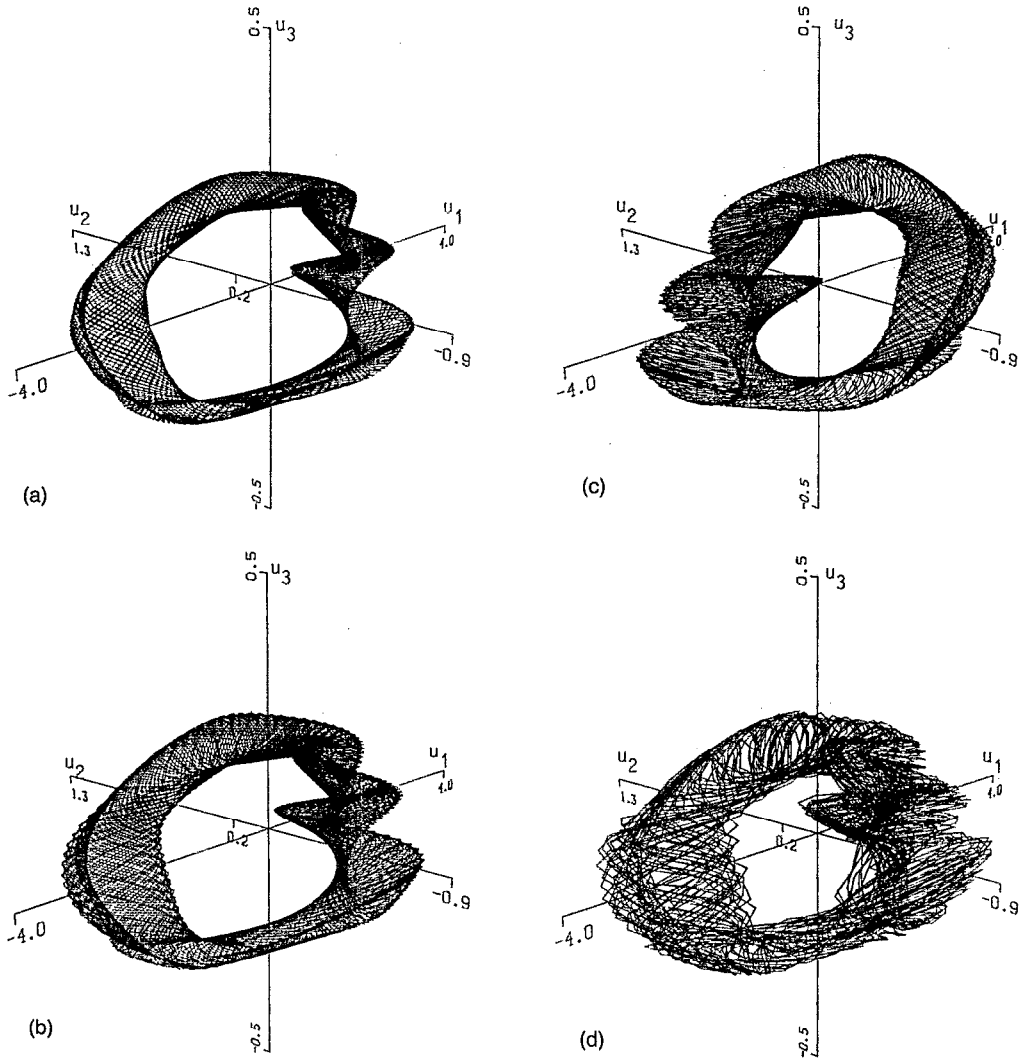

FIG. 6. A transition from quasiperiodic to chaos, five modes. (a) $e=2.8$; (b) $e=2.75$; (c) $e=2.7$; and (d) $e=2.65$.

pressure fluctuations at the outer edge of the boundary layer), then the interval between spikes can be made to become bounded. Since the pressure fluctuations were neglected in their model, they argue that the fluctuating pressures from the outer boundary layer trigger the bursts.

In view of the results presented thus far the origin of the bursts requires further investigation. In this regard two remarks deserve mention. First, it is clear from our deliberations in Secs. II and III, that both the fluctuating pressure and the velocity at the outer edge of the wall region can affect the flow. Specifying the pressure alone at the outer edge of the wall region is not sufficient to solve the flow problem in the wall region. Two additional boundary conditions are required for a well-posed formulation. Second, as will be seen in Sec. X, adding modes with streamwise variations to the model equations changes the behavior in an essential way. If bursting needs a trigger there are sound reasons to believe that it is furnished by certain neglected modes with streamwise variations. In the Cornell model, it was noted that maximum amplitudes of pressure fluctuations are two orders of magnitude smaller than the maximum amplitudes of the variables A_i. As we will see in the next section, neglected modes with streamwise variations are the same order of the modes we kept so far and play a more important role.

IX. PROPAGATING AND NONPROPAGATING MODES

In examining the structures in the full simulation of turbulent channel flows, it was found that two classes emerged; propagating modes and nonpropagating modes.[26,27] This we now briefly review. As discussed earlier, the eigenfunctions factor into Fourier components in the streamwise and spanwise directions due to homogeneity, but take on a more complicated form in the wall normal direction. For each mode, one streamwise wave number, k_1, one spanwise wave number, k_3, and one vertical quantum number, q, enter. The projection of a flow along a channel eigenfunction,

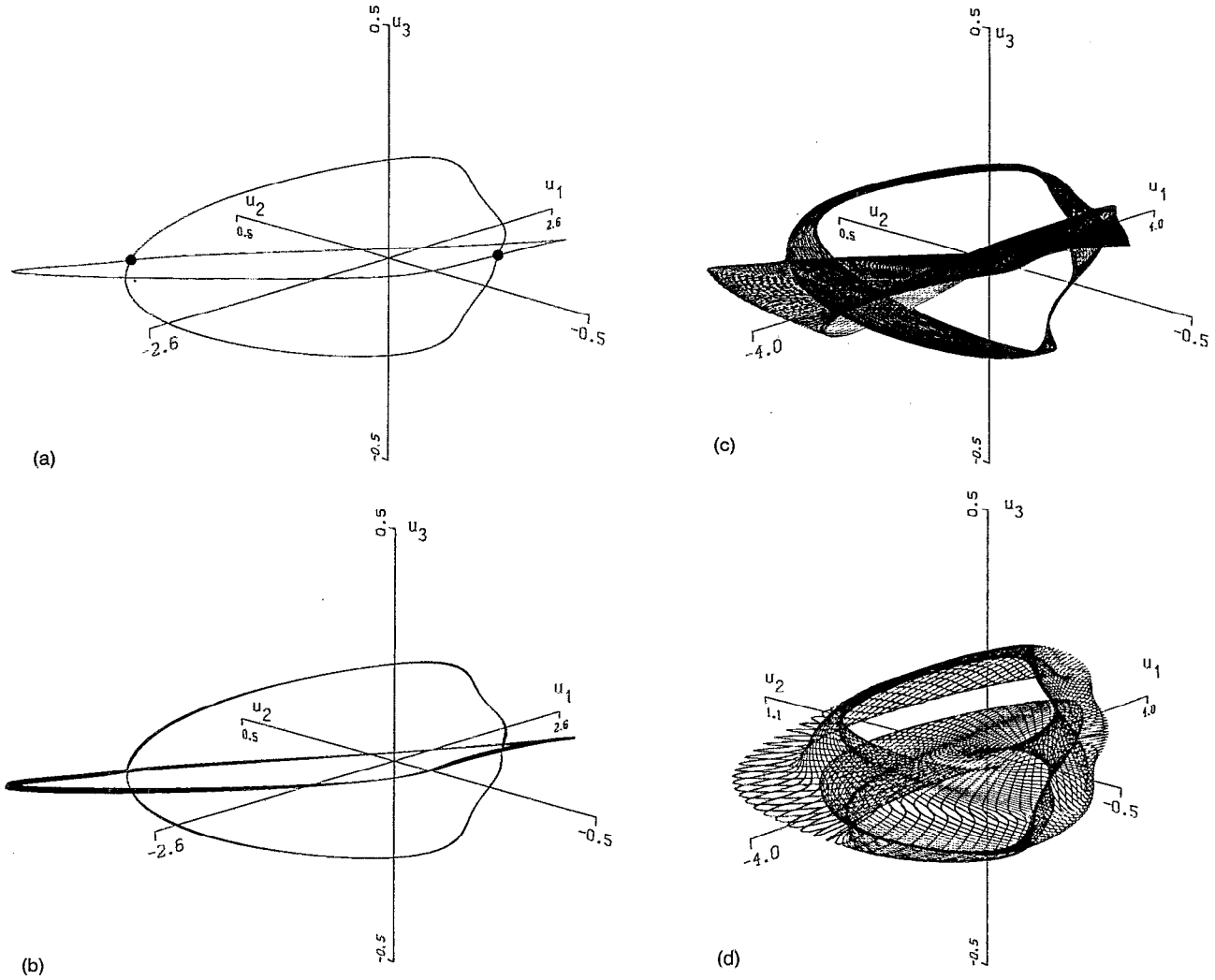

FIG. 7. A demonstration of a heteroclinic cycle and the transition to quasiperiodic solution, five modes, the same initial conditions as in Fig. 5 are chosen. (a) $e=4.6$, heteroclinic loop and equilibrium points. (b) $e=4.5$, (c) $e=4.45$, (d) $e=4.3$.

$$A_{\mathbf{k}}^{(q)}=(\mathbf{V}_{\mathbf{k}}^{(q)},\mathbf{u}), \tag{71}$$

furnishes a time history of the mode amplitude, and its phase is defined by

$$\theta_{\mathbf{k}}^{(q)}=\tan^{-1}[\mathrm{Im}(A_{\mathbf{k}}^{(q)})/\mathrm{Re}(A_{\mathbf{k}}^{(q)})], \tag{72}$$

and from it the frequency is given by

$$\omega_{\mathbf{k}}^{(q)}=\lim_{t\to\infty}\theta_{\mathbf{k}}^{(q)}/t. \tag{73}$$

It was then determined from the simulation that for all significant modes,

$$\omega_{k_1,k_3}^{(q)}\neq 0, \quad k_1\neq 0 \tag{74}$$

and

$$\omega_{0,k_3}^{(q)}=0. \tag{75}$$

The modes corresponding to (74) are termed propagating and the modes in (75) nonpropagating or degenerate. The contribution of the propagating modes to the fluctuating velocity can then be written as

$$V_j^{(q)}=b_{\mathbf{k}}^{(q)}(t)\psi_j^{(q)}e^{i(\omega_{\mathbf{k}}^{(q)}t+\mathbf{k}\cdot\mathbf{x}')}, \tag{76}$$

here $\mathbf{x}'=2\pi(x_1/L_1,x_3/L_3)$ and $b_{\mathbf{k}}^{(q)}(t)$ is the amplitude of $A_{\mathbf{k}}^{(q)}$. Clearly, (76) has the form of a propagating plane wave when (74) holds. The coefficient, $b_{\mathbf{k}}^{(q)}(t)$, exhibits the irregular temporal behavior that is typical of variables found in turbulent flows.

In the cited references, arguments were presented, which indicate that the propagating modes act as triggers in the bursting process.

X. EMPIRICAL DYNAMICAL SYSTEMS WITH PROPAGATION

Our goal in this section is to produce more realistic models based on the inclusion of propagating modes and by virtue of this to include three-dimensionality.

We begin with the general ordinary differential equations (49) and continue to adopt the eddy viscosity model. To obtain reduced systems, we only add the quantum numbers equal to one mode ($q=1$). The relation $g_{mn}(\mathbf{k})=g_{11}(\mathbf{k})=1$ remains true. If we set $A_{\mathbf{k}} = a^1_{\mathbf{k}}$, the equations take the form

$$\frac{dA_{\mathbf{k}}}{dt}=L(\mathbf{k},\mathrm{Re}_*)A_{\mathbf{k}}+\sum_{k'} Q(\mathbf{k}',\mathbf{k})A_{\mathbf{k}'}A_{\mathbf{k}-\mathbf{k}'}$$

$$-\mathrm{Re}_*\sum_{\mathbf{k}'} C(\mathbf{k}',\mathbf{k})A_{\mathbf{k}}|A_{\mathbf{k}'}|^2. \qquad (77)$$

In the numerical studies, we focus on a 16-mode model, in which the modes with $k_1=0$, $k_3=1,...,5$ and $k_1=1$, $k_3=0$, $\pm 1,...,\pm 5$ are included. For comparison, we also include results from a 27-mode model, in which the modes with $k_1=0$, $k_3=1,...,5$ and $k_1=1,2$, $k_3=0$, $\pm 1,...,\pm 5$ are included. The propagating modes included in these groupings correspond to the most important found in Refs. 26 and 27. The *importance* here is not solely based on energy content, but the ability to interact with the main energy bearing modes, which corresponds to $k_1=0$. These important propagating modes are best able to interact with the energy modes.

TABLE II. A summary of numerical integrations.

Eddy viscosity	Behavior
$14.0>e>4.6$	Intermittency
$4.6>e>4.2$	Transition from intermittency to chaotic and quasiperiodic solutions
$4.2>e>0$	Chaos, quasiperiodic solutions

Through numerical integration, we have found that

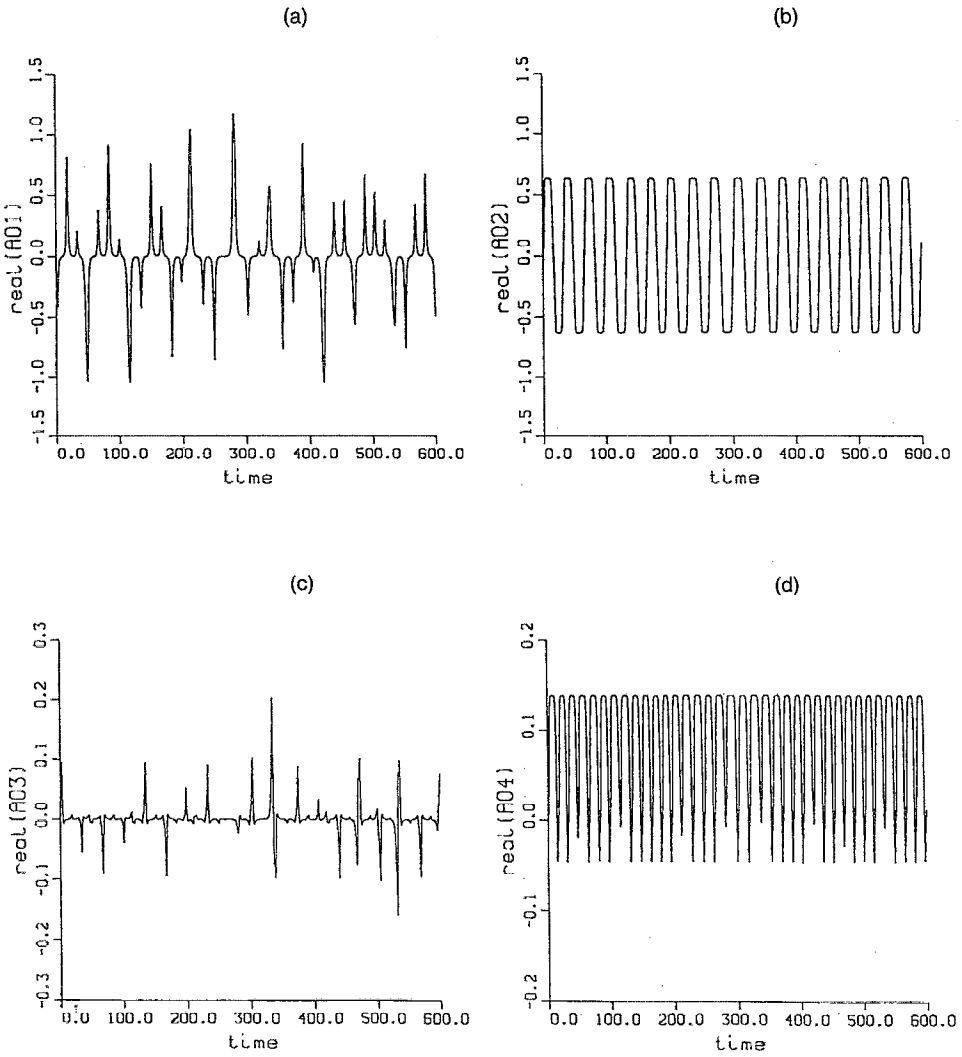

FIG. 8. Irregular intermittency, 16 modes, $e=4.6$. (a) real(A_{01}); (b) real(A_{02}); (c) real(A_{03}); (d) real(A_{04}); (e) real(A_{11}); (f) real($A_{1,-1}$); (g) velocity; (h) the power spectrum of (g); and (i) three velocity components.

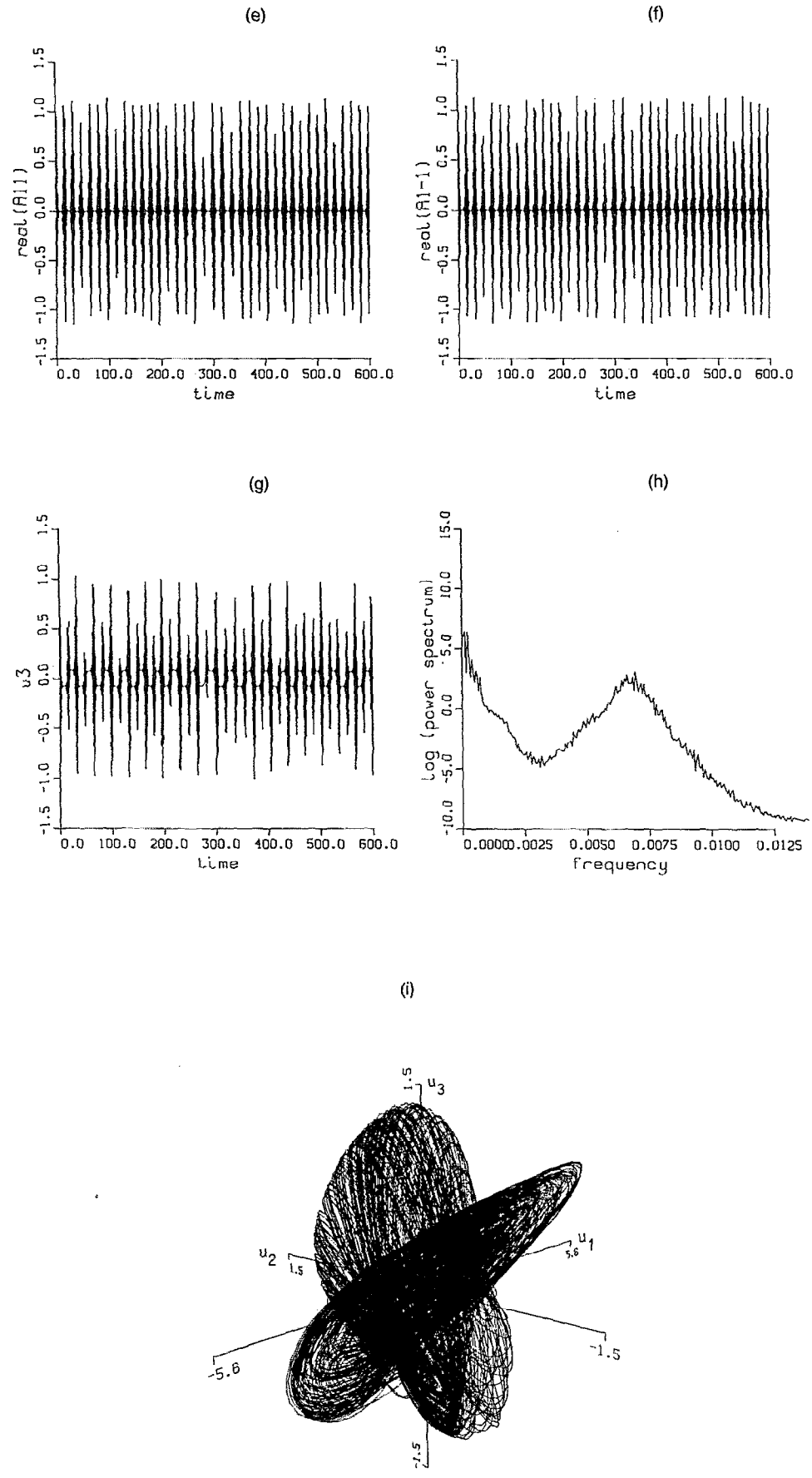

FIG. 8. (*Continued.*)

our model equations display intermittent, quasiperiodic, and chaotic behavior. A summary of the numerical integrations of the 16-mode equations is given in Table II.

For large enough values of e, all propagating modes are damped to zero. As before, we chose to stop at $e=14$. When $14>e>4.6$, intermittent solutions occur; the time history of mode A_{01} is comprised of spikes, as before; A_{02} oscillates between two nonzero steady states, and so forth. The propagating modes all vibrate chaotically. Figures 8 show the results. The time trace of A_{01} resembles what was earlier called irregular intermittency. However, the propagating modes are clearly chaotic, and the power spectrum shown in Fig. 8(h) verifies this. (If the eddy viscosity is increased to $e=5$ the picture closely resembles the case of regular intermittency discussed earlier.) In Fig. 9 we show a more violently chaotic case and in Fig. 10 we show a transition from a quasiperiodic to a chaotic solution, which appears to follow the Ruelle–Takens–Newhouse route,[41] i.e., first there is a torus, then it becomes unstable and chaos appears.

The power spectra of the intermittent and chaotic solutions have two peak frequencies [see Figs. 8(h), 9(h), and 10(d)]. We term the high-frequency peak the *preferred frequency*, which results from the presence of propagating modes.

If we compare the numerical results of 16 modes and 5 modes, it is clear that adding the propagating modes to the five-mode equations changes the solutions in an essential way. It is interesting to observe that the propagating modes change the regular intermittency to an irregular one (compare Figs. 3 and 8). Comparison of the phase spaces shown in Figs. 7(a) and 8(i) shows that a dramatic change occurs when the propagating modes are added to the model.

Figure 11 shows some statistical results, which follow from our 16 model equations, at $e=4.1$, and compare this with the data from the original full simulation.[15] The max-

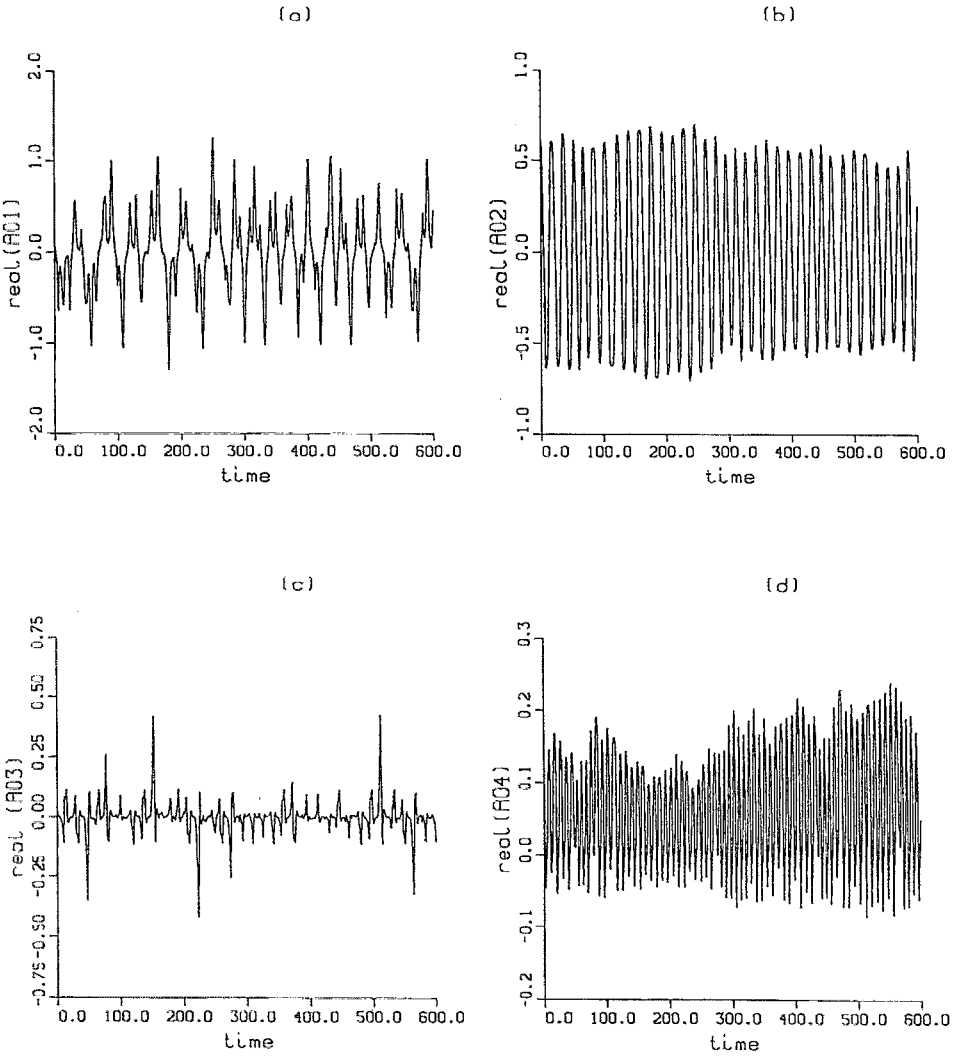

FIG. 9. Chaos, 16 modes, $e=4.1$. (a) real(A_{01}); (b) real(A_{02}); (c) velocity, real(A_{03}); (d) real(A_{04}); (e) real(A_{11}); (f) real($A_{1,-1}$); (g) velocity; and (h) the power spectrum of (g).

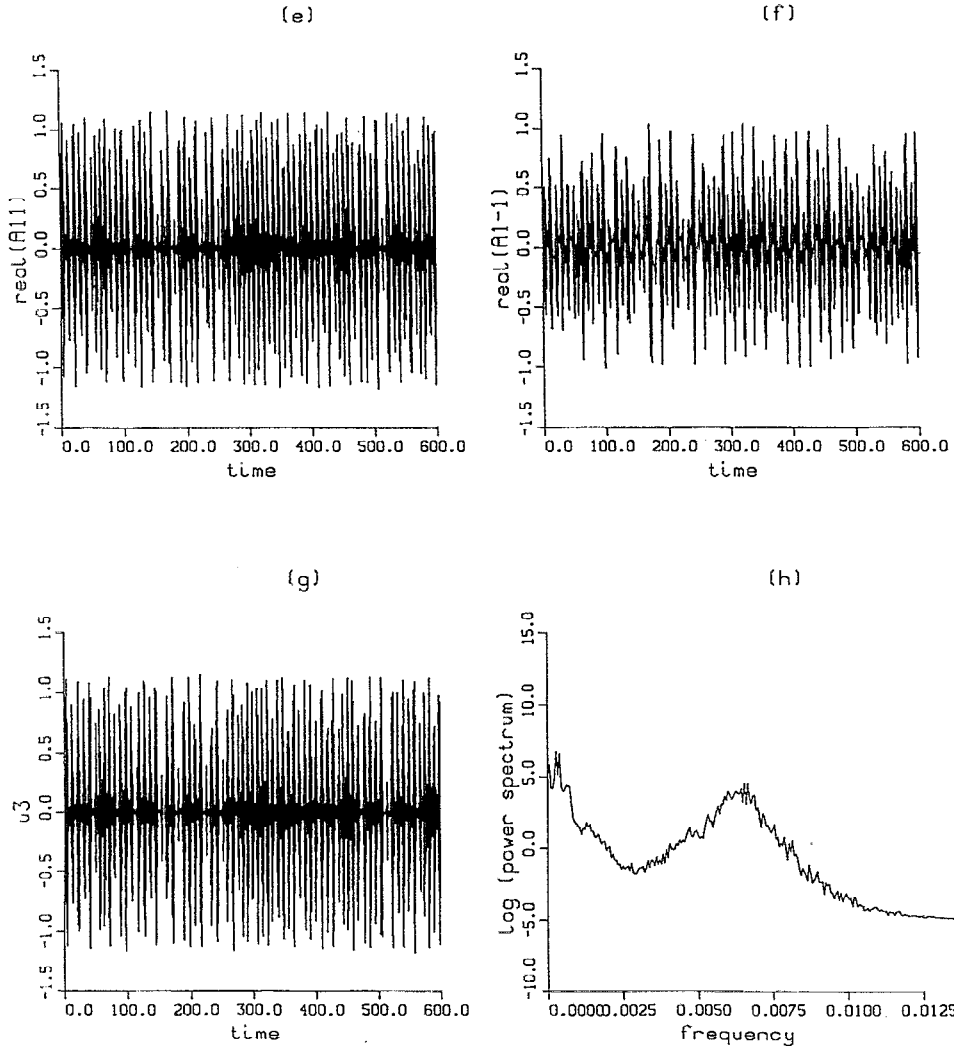

FIG. 9. (*Continued.*)

imum of the Reynolds stress, $-\overline{uv}$, appears at $x_2 \approx 30^+$, and the maximum of the $u_{\rm rms}$, root of mean square velocity of the streamwise component, appears at $x_2 = 15^+$. The location of the peaks fall almost exactly on the values from the original full direct numerical simulation. The maximum of $u_{\rm rms}$ itself, however, is larger than the *correct* value and $v_{\rm rms}$ is below the exact curve; the Reynolds stress, $-\overline{uv}$, is also smaller than the correct values. This occurs since the streamwise components of the KL eigenfunctions involved are much larger than the normal components, and only relatively few modes are included. The instantaneous Reynolds stress is plotted in Fig. 12.

Modes for which $k_1 = 1$ show propagation in all the cases we consider. In Fig. 13 we plot the time courses of the magnitudes and phases of $A_{\rm k}$ with $\mathbf{k} = (1, k_3)$. Although the amplitudes change with time chaotically, the phase shows a secular linear decrease. The difference between the curve and a strict straight line is too small to be seen. Contributions of such modes to the fluctuating velocity can thus be expressed as (76), i.e., they are propagating modes. As mentioned above,[26,27] these propagating wave structures appear in large-scale simulations of wall bounded turbulent flow.

The frequency associated with one of the propagating modes ($k_1 = 1$), defined by (73), exhibits itself in the spectrum as the preferred frequency. To illustrate this we plot the power spectrum for the five-mode dynamic system in Fig. 14 for comparison with Figs. 8(h), 9(h), and 10(d). It can be seen that the preferred frequency disappears in Fig. 14. To further indicate that the frequencies of propagating waves show themselves in the power spectra as preferred frequencies, we also show the result of integrating a 27-mode system, in which the modes with streamwise wave number $k_1 = 2$ are also included. As shown in Fig. 15, another preferred frequency appears. The ratio of two frequencies is roughly two. It is anticipated that as more propagating modes are included in the dynamic equations,

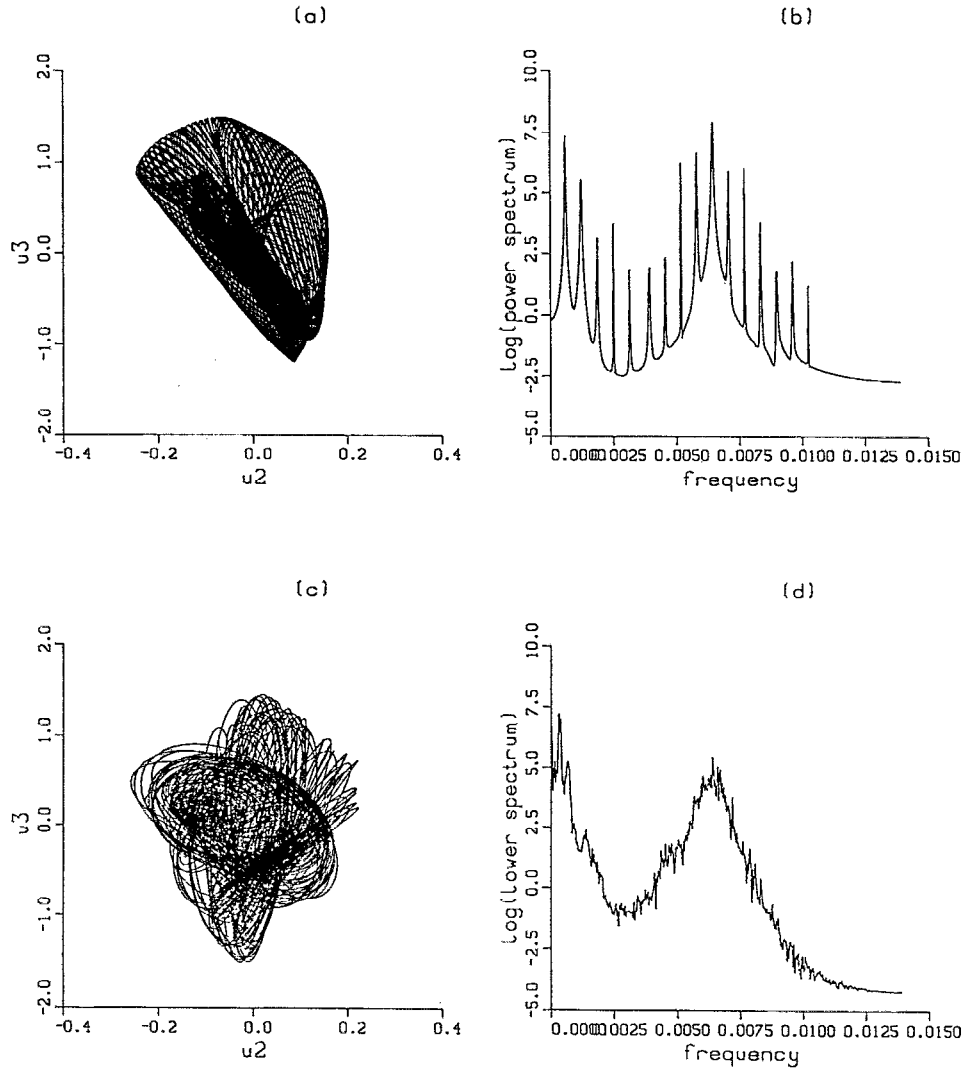

FIG. 10. A transition from quasiperiodic solution to chaos, 16 modes. (a) Quasiperiodic solution at $e=4.07$; (b) the power spectrum of u_2; (c) chaos at $e=4.09$; and (d) the power spectrum of u_2.

more peaks will appear on power spectra. An indication of this has been observed in experiments.[31]

XI. CONCLUSIONS

By developing a method for the construction of "wall" eigenfunctions with full channel validity, it has been possible to avoid the unknown inhomogeneous terms. The methodology is not restricted to the channel flow, and we can envision employing the procedures presented here in a variety of other turbulent flows.

Our investigation of the five mode system appears to confirm the presence of heteroclinic cycles. From the study of 16- and 27-mode model equations, we find that propagating and nonpropagating modes, which appear in the full simulations,[26,27] also exist in these much smaller systems. This result has inspired us to further investigate dynamical equations including any number of modes and discover general periodic solutions. The discovery can be used to explain some results from the full simulations in Refs. 26 and 27. The investigation will be presented elsewhere.

By enriching the model with the addition of key propagating modes the bursting process is altered in an essential way. The resulting "small" systems comprised of 16 and 27 modes show remarkable qualitative agreement with full simulations. It appears that the propagating modes lie more at the heart of the triggering mechanism for the bursting process than does the idea of pressure fluctuations. One can now hope to deal with the mechanisms for bursting, as found in small systems. For example, the notion of control can be considered within this framework.

The idea of propagating waves can also be associated with ideas from transition theory. As mentioned in Refs. 26 and 27, propagating modes, the most significant of which propagate at an angle of roughly 65° to the stream direction, bear a strong resemblance to the secondary waves of stability theory, which are known to trigger instability in laminar flows.[42–44] Therefore there is a strong

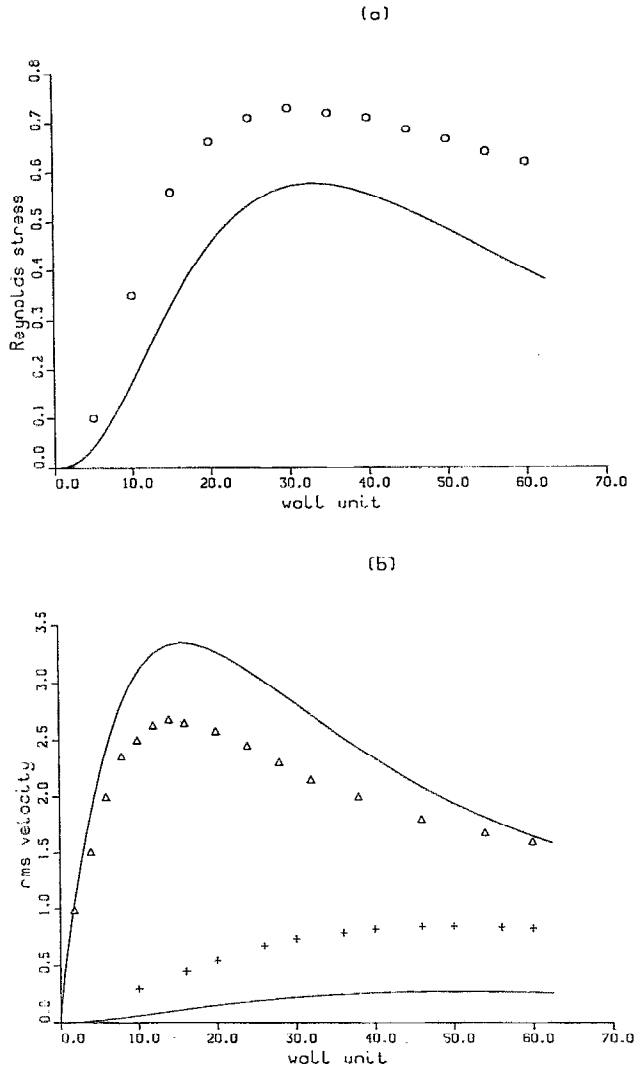

FIG. 11. A comparison of the statistics with the full simulation; data from the original simulation are marked; the solid lines are from 16 modes at $e=4.6$. (a) Average Reynolds stress $-uv$; (b) root mean square velocity of streamwise component, $u_{\rm rms}$, and normal component, $v_{\rm rms}$.

physical suggestion that oblique waves are a necessary mechanism in the process. Both the 16- and 27-mode dynamical systems contain these traveling waves and generate behavior closer to reality. Five-mode theory, on the other hand, lacks this essential feature since it contains no streamwise variation.

ACKNOWLEDGMENTS

The authors gratefully acknowledge the use of the Pittsburgh Supercomputing Center. The authors thank Ken Ball for generously providing the full channel eigenfunctions and other significant data. Thanks are also due to P. Holmes and E. Stone for their comments on an earlier version of this paper. Finally, we express grateful appreciation to Chris Jones for valuable discussions and suggestions.

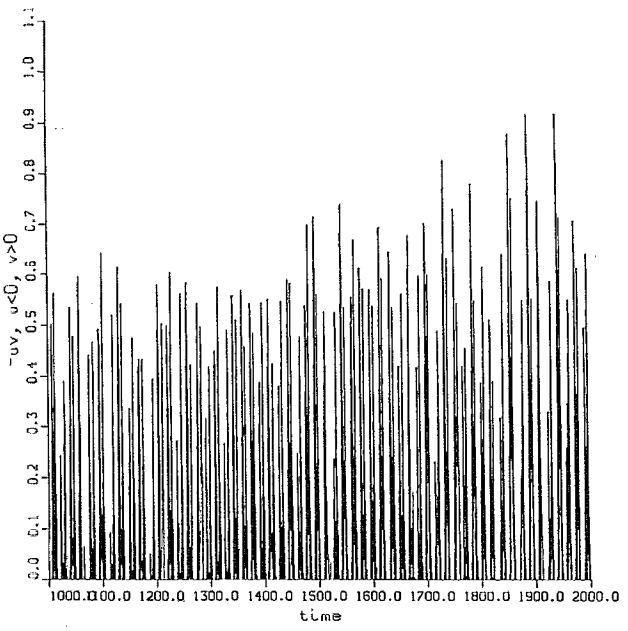

FIG. 12. The instantaneous Reynolds stress at $e=4.1$, 16 modes.

This work was supported by Office of Naval Research (ONR) Contract No. N00014-91-J-1588 and the National Science Foundation, NSF IRI-91-645.

APPENDIX: NUMERICAL COEFFICIENTS

The numerical values of coefficients in (66) are the following:

Linear terms,

$$\mathbf{L}^{(1)} = -(0.308, 0.524, 1.037, 1.640, 2.447),$$

$$\mathbf{L}^{(2)} = (7.07, 12.34, 16.19, 19.91, 20.66);$$

quadratic terms,

$$(Q_{-12}, Q_{-23}, Q_{-34}, Q_{-45}) = (0.837, 1.392, 2.225, 2.779),$$

$$(Q_{-13}, Q_{-24}, Q_{-35}, Q_{11}) = (1.319, 1.593, 2.501, -0.228),$$

$$(Q_{-14}, Q_{-25}, Q_{12}) = (1.843, 2.190, -0.521),$$

$$(Q_{-15}, Q_{13}, Q_{22}) = (2.240, -0.878, -0.676),$$

$$(Q_{14}, Q_{23}) = (-1.279, -0.992);$$

and cubic terms,

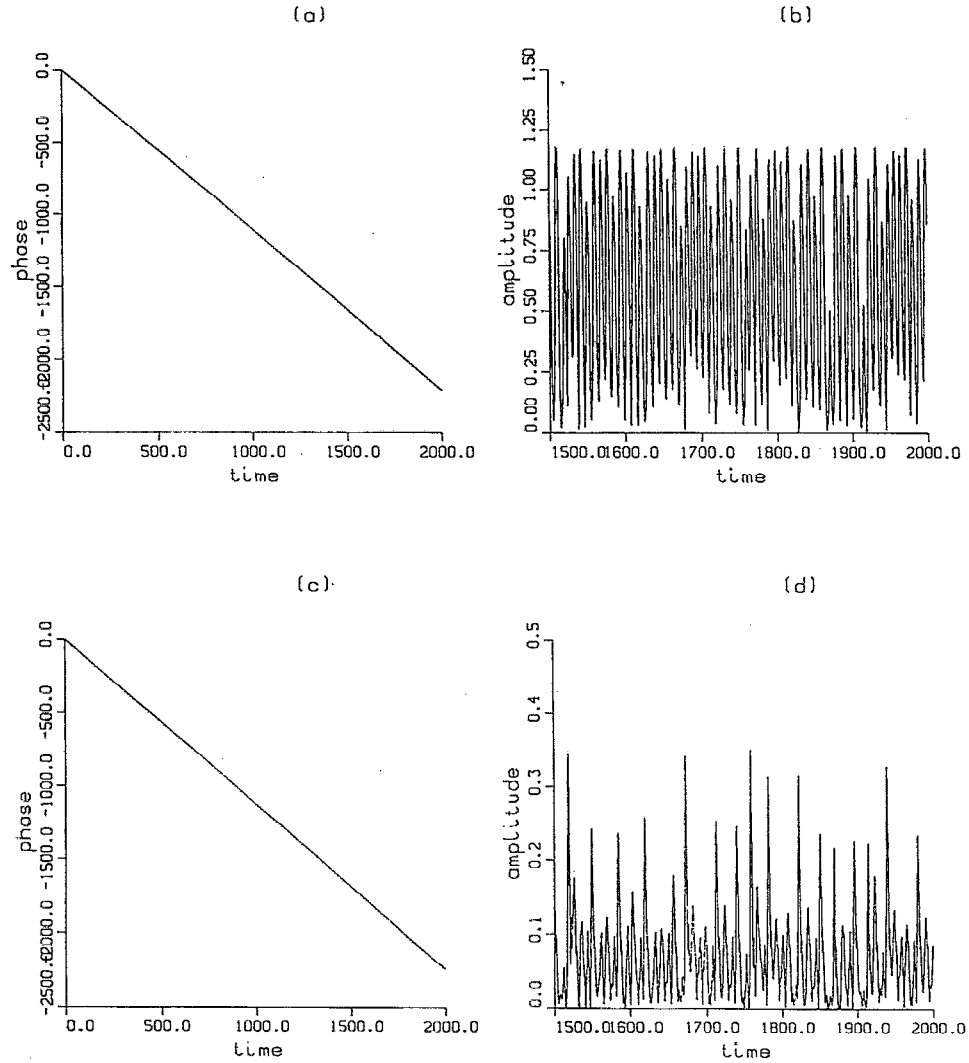

FIG. 13. Phases and amplitudes of some propagating modes, 16 modes, $e=4.1$. (a) The phase of the A_{11} mode; (b) the amplitude of the A_{11} mode; (c) the phase of the A_{12} mode; and (d) the amplitude of the A_{12} mode.

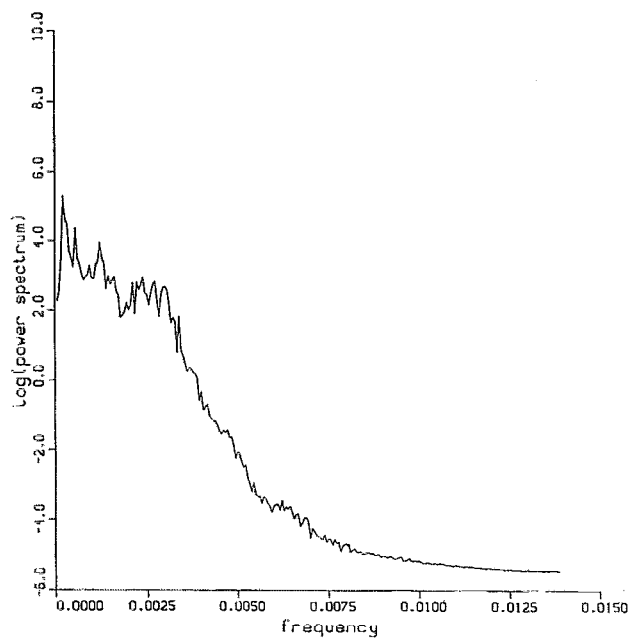

FIG. 14. A power spectrum of u_2, five modes, $e=2.5$.

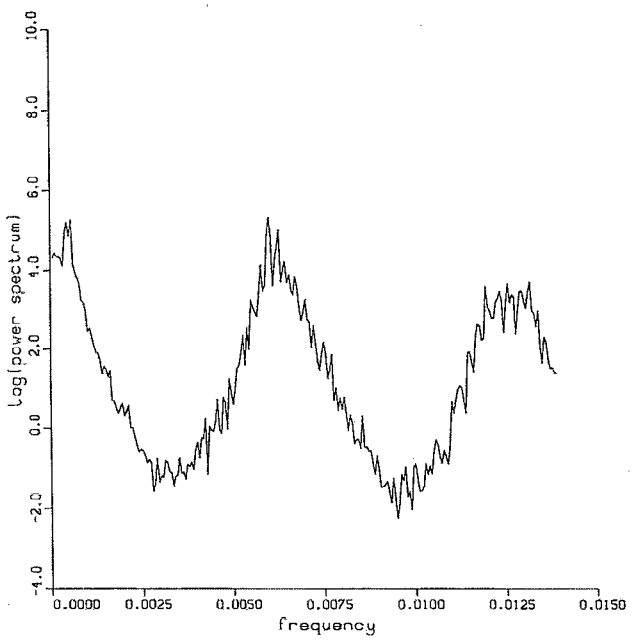

FIG. 15. A power spectrum of u_2, 27 modes, $e=4.1$.

$$\mathbf{C}=\begin{pmatrix} 2.198 & 3.414 & 4.315 & 4.640 & 4.738 \\ 3.414 & 5.784 & 7.678 & 8.531 & 8.679 \\ 4.315 & 7.678 & 10.92 & 12.95 & 13.42 \\ 4.640 & 8.531 & 12.95 & 16.56 & 17.54 \\ 4.738 & 8.679 & 13.42 & 17.54 & 18.87 \end{pmatrix}.$$

Note, all the numerical integrations of ordinary differential equations (ODE's) were done on the Cray of Pittsburgh Supercomputing Center. A sixth-order Runge–Kutta method with step size 0.01 is employed. The results are taken after the first 20 000 steps. If not otherwise stated, the initial values for the integrations are $A_k = [\cos(0.5*k),\sin(0.5*k)]$, with $k=1,2,\ldots,K$. The values of the parameters are from the original simulation, i.e., $\mathrm{Re}_* = u_* H/\nu = 180$, $L_1 = 4\pi$, and $L_3 = 4\pi/3$.

[1]W. W. Wilmarth, "Structures of turbulence in boundary layers," Adv. Appl. Mech. **15**, 159 (1975).

[2]W. W. Wilmarth, "Pressure fluctuations beneath turbulent boundary layers," Annu. Rev. Fluid Mech. **7**, 13 (1975).

[3]J. P. Kim, P. Moin, and R. D. Moser, "Turbulence statistics in fully developed channel flow at low Reynolds number," J. Fluid Mech. **177**, 133 (1987).

[4]S. J. Kline, W. C. Reynolds, F. A. Schraub, and P. W. Rundstadler, "The structure of turbulent boundary layers," J. Fluid Mech. **30**, 741 (1967).

[5]S. Herzog, "The large scale structure in the near-wall region of turbulent pipe flow," Ph.D. thesis, Cornell University, 1986.

[6]H. T. Kim, S. J. Kline, and W. C. Reynolds, "The production of turbulence near a smooth wall in a turbulent boundary layer," J. Fluid Mech. **50**, 133 (1971).

[7]E. R. Corino and R. S. Brodkey, "A visual investigation of the wall region in turbulent flow," J. Fluid Mech. 37, 1 (1969).

[8]L. Sirovich, "Chaotic dynamics of coherent structures," Physica D **37**, 126 (1989).

[9]L. Sirovich, "Turbulence and the dynamics of coherent structures, Part I–III," Q. Appl. Math. **XLV**, 561 (1987).

[10]K. Ball, L. Sirovich, and L. Keefe, "Dynamical eigenfunction decomposition of turbulent channel flow," Int. J. Num. Methods Fluids **12**, 585 (1991)

[11]L. Sirovich and J. D. Rodriguez, "Coherent structures and chaos: A model problem," Phys. Lett. A **120**, 211 (1987).

[12]D. H. Chambers, R. J. Adrian, P. Moin, D. S. Stewart, and H. J. Sung, "Karhunen–Loève expansion of Burgers' model of turbulence," Phys. Fluids **31**, 2573 (1988).

[13]A. V. Tangborn, L. Sirovich, and C. L. Streett, "An orthogonal decomposition of finite length chaotic Taylor–Couette flow," Bull. Am. Phys. Soc. **33**, 2242 (1988).

[14]T. Howes, L. Sirovich, and T. A. Zang, "Eigenfunction analysis of Rayleigh–Bénard convection," Bull. Am. Phys. Soc. **33**, 2261 (1988).

[15]P. Moin and R. D. Moser, "Characteristic-eddy decomposition of turbulence in a channel," J. Fluid Mech. **200**, 471 (1988).

[16]A. E. Dean and C. Mavriplis, "Low-dimensional description of the dynamics in separated flow past thick airfoils," *AIAA 22nd Fluid Dynamics, Plasma Dynamics, and Lasers Conference*, June, 1991 (AIAA, Washington, DC, 1992).

[17]A. E. Deane, I. G. Kevrekidis, G. E. Karniadakis, and S. A. Orszag, "Low-dimensional models for complex geometry flows. Application to channels and circular cylinders," Phys. Fluids A **3**, 2337 (1991).

[18]C. C. Chen and H. C. Chang, "Accelerated disturbances damping of an unknown distributed system by nonlinear dominant-mode feedback," AIChE J. **38**, 1461 (1992).

[19]R. W. Preisendorfer, *Principal Component Analysis in Meteorology and Oceanography* (Elsevier, New York, 1988).

[20]L. Sirovich and R. Everson, "Management and analysis of large scientific datasets," Int. J. Supercomput. Appl. **6**, 50 (1992).

[21]E. N. Lorenz, "Empirical orthogonal functions and statistical weather prediction," Scientific Rep. No. 1, Statistical Forecasting Project, Massachusetts Institute of Technology, Department of Meteorology, 1956, p. 49.

[22]J. E. Kutzbach, "Empirical eigenfunctions of sea-level pressure, surface temperature and precipitation complexes over North America," J. Appl. Meteorol. **6**, 791 (1967).

[23]A. M. Obukhov, "On the dynamics of a stratified fluid," Dokl. Akad. Nauk. SSSR **145**, 1239 (1962).

[24]J. L. Lumley, "The structure of inhomogeneous turbulent flows," *Atmospheric Turbulence and Radio Wave Propagation*, edited by A. M. Yaglom and V. I. Tatarski (Nauka, Moscow, 1967).

[25]N. Aubry, P. Holmes, J. L. Lumley, and E. Stone, "The dynamics of coherent structures in the wall region of turbulent boundary layer," J. Fluid Mech. **192**, 115 (1988).

[26]L. Sirovich, K. S. Ball, and L. R. Keefe, "Plane waves and structure in turbulent channel flow," Phys. Fluids A **2**, 2217 (1990).

[27]L. Sirovich, K. S. Ball, and R. A. Handler, "Propagating structures in wall-bounded turbulent flows," Theor. Comput. Fluid Dyn. **2**, 307 (1991).

[28]W. R. B. Morrison, K. J. Bullock, and R. E. Kronauer, "Experimental evidence of waves in the sublayer," J. Fluid Mech. **47**, 639 (1971).

[29]K. Ball (private communications, 1989).

[30]N. Aubry and S. Sanghi, in *Turbulence and Coherent Structures*, edited by O. Metais and M. Lesieur (Kluwer Academic, New York, 1991).

[31]K. Ball, D. G. Bogard, and C. Gan (private communication, 1991).

[32]L. Sirovich, J. D. Rodriguez, and B. Knight, "Two boundary value problems for the Ginzburg Laudau equation," Physica D **43**, 63 (1990).

[33]R. B. Ash and M. F. Gardner, *Topics in Stochastic Processes* (Academic, New York, 1975).

[34]N. Aubry, "On the hidden beauty of the proper orthogonal decomposition." Theor. Comput. Fluid Dyn. **2**, 339 (1991).

[35]C. Foias, O. Manley, and L. Sirovich, "Empirical and Stokes eigenfunctions and the far-dissipative turbulent spectrum," Phys. Fluids A **2**, 462 (1990).

[36]R. Courant and D. Hilbert, *Methods of Mathematical Physics* (Interscience, New York, 1958), Vol. 1.

[37]D. Armbruster, J. Guckenheimer, and P. Holmes, "Heteroclinic cycles and modulated traveling waves in systems with $O(2)$ symmetry," Physica D **29**, 257 (1988).

[38]E. Stone and P. Holmes, "Noise-induced intermittency in a model of a turbulent boundary layer," Physica D **37**, 20 (1989).

[39]J. Guckenheimer and P. Holmes, *Nonlinear Oscillations, Dynamical Systems and Bifurcations of Vector Fields* (Springer-Verlag, New York, 1983).

[40]S. Wiggins, *Global Bifurcations and Chaos* (Springer-Verlag, New York, 1988).

[41]S. Newhouse, D. Rulle, and F. Takens, "Occurence of stange axiom-A attractors near quasiperiodic flow on T^m, $m<3$," Commun. Math. Phys. **64**, 35 (1978).

[42]D. S. Henningson and J. Kim, "On turbulent spots in plane Poiseuille flow," J. Fluid Mech. **228**, 183 (1991).

[43]T. Herbert, "Secondary instability of boundary layers," Annu. Rev. Fluid Mech. **20**, 487 (1988).

[44]S. A. Orszag and L. C. Kells, "Transition to turbulence in plane Poiseuille and Couette flow," J. Fluid Mech. **96**, 159 (1980).